Final report for Living Planet Fellowship: The ionospheric signature of auroral and subauroral fast flows

Dr. William E. Archer

The intent of this fellowship was to investigate auroral and subauroral fast flows with the Swarm satellites. The high-resolution Electric Field Instruments (EFI) on the Swarm satellites provide a unique opportunity to investigate small-scale flow structures that are often below the resolution of ground-based radars. The orbits of the Swarm satellites (polar orbits that precess in magnetic local time (MLT)) allow the Swarm mission to at times sample regions that have not been thoroughly investigated with similar instrumentation, namely near magnetic noon and midnight. Over the past two years this investigation has taken the form of 4 distinct studies, two of which are currently published. In this report I will provide a high-level summary of each of these studies and attach more in-depth descriptions of the research as appendices.

1) Steve: The Optical Signature of Intense Subauroral Ion Drifts:

In this study we use coincident ground-based optical measurements and Swarm satellite measurements to establish a link between subauroral ion drifts (SAID), and the recently coined optical signature "Steve". Not only did we consistently observe the ionospheric signature SAID coincident with the optical signature of Steve, but the SAID we observed were unusually intense, with very large flow velocities and electron temperatures, and very low plasma densities. These extreme plasma parameters (when compared with typical SAID) imply a causal link between intense SAID and Steve and suggest that Steve may be caused by these plasma conditions. Until such a time that a clear counterexample to our suggested link between SAID and Steve can be found, this manuscript will remain a foundational piece of research in the study of Steve. This research provides some clear constraints on potential mechanisms for Steve based on the high-quality in-situ plasma measurements made by the Swarm satellites.

The publication on this research has been sited 10 times in the past year, was among the top 10% most-read papers published by Wiley publishing in 2019, and can has been attached to this document as **Appendix A**.

2) The vertical Distribution of the Optical Emissions of a Steve and Picket Fence Event:

In this study we use coincident optical observations of a Steve and "picket fence" event taken by amateur auroral photographers to triangulate the altitude distribution of these two phenomena. We show the picket fence to extend between 95 and 150 km, while Steve spans between 130 and 270 km altitude. While this research was not particularly technically complicated, great care was required in identifying and processing ideal observations. These altitude estimates have been reproduced by many

different researchers since their publication and provide clear constraints on possible physical mechanisms that could be responsible for Steve and the "picket fence".

The publication on this research has been sited 9 times in the past year, was among the top 10% most-read papers published by Wiley publishing in 2019, and can has been attached to this document as **Appendix B**.

3) Neutral Atmospheric Signature of Birkeland Current Boundary Flows:

In this study we use neutral atmospheric density estimates from the Swarm satellites to investigate potential neutral upwelling caused by Birkeland Current Boundary Flows (BCBF). BCBF are narrow and intense auroral flow channels, and as such are likely to cause some neutral upwelling because of frictional heating. Although the Swarm accelerometer dataset can be challenging to work with, this project was proposed because significant small-scale neutral density enhancements should produce a clear signature so long as they are not co-located with an instrument artifact measurement discontinuity. As expected, working with the Swarm accelerometer measurements provided significant challenges. However, we successfully identified a neutral density signature that persists for 6 orbits and appears to be associated with a BCBF event.

At this point additional research is required to separate geophysical signatures from potential instrument artifacts in order to formalize what can and cannot be interpreted from these observations. To this end, I look forward to working with Dr. Elizabetta Iorfida to convert the current state of the research (provided as **Appendix C**) into a publication.

4) Investigation of highly correlated electric and magnetic perturbations

In this case study we investigate extremely unusual measurements by the Swarm satellites taken on 26 February 2014. In this event we observe highly structured electric and magnetic perturbations with a spatial scale of around 150km. The electric and magnetic perturbations correlate to an incredibly high degree (correlation coefficient of 0.94), which is unusual for such a structured and likely dynamic region. The current analysis focuses on distinguishing whether the observed structure is due to Alfvenic activity or static but structured sheet currents. As the observations to not appear to clearly match either description, additional research is required.

The current state of the research is provided as **Appendix D**.

Closing thoughts

I believe that this Living Planet Fellowship was successful in leveraging ESA satellite measurements to advance ionospheric physics. Two of the four projects of this fellowship resulted in highly read and cited publications, and I expect to publish the results of the remaining two projects in the near future. I would like to take this opportunity to thank all those at ESA involved in this program for the opportunities that this fellowship provided me. Particularly in this past year, working on this fellowship provided stability and consistency in an otherwise tumultuous time.

I look forward to working with you in the future,

Dr. William Edward Archer

Geophysical Research Letters

RESEARCH LETTER
10.1029/2019GL082687

Key Points:
- Eight Steve events were identified in all-sky imager measurements with coincident or near-coincident measurements from the Swarm satellites
- In all cases, evidence of subauroral ion drifts are observed in Swarm measurements
- All measurements of SAID overlapping with Steve have very fast ion flows, high electron temperatures, and extremely low plasma densities

Supporting Information:
- Supporting Information S1

Correspondence to:
W. E. Archer,
wea784@mail.usask.ca

Citation:
Archer, W. E., Gallardo-Lacourt, B., Perry, G. W., St.-Maurice, J.-P., Buchert, S. C., & Donovan, E. F. (2019). Steve: The optical signature of intense subauroral ion drifts. *Geophysical Research Letters*, *46*, 6279–6286. https://doi.org/10.1029/2019GL082687

Received 4 MAR 2019
Accepted 28 MAY 2019
Accepted article online 4 JUN 2019
Published online 26 JUN 2019

Steve: The Optical Signature of Intense Subauroral Ion Drifts

W. E. Archer[1], B. Gallardo-Lacourt[2], G. W. Perry[2,3], J. P. St.-Maurice[1,4], S. C. Buchert[4,5], and E. Donovan[2]

[1]Department of Physics and Engineering Physics, University of Saskatchewan, Saskatoon, Saskatchewan, Canada, [2]Department of Physics and Astronomy, University of Calgary, Calgary, Alberta, Canada, [3]Center for Solar-Terrestrial Research, New Jersey Institute of Technology, Newark, NJ, USA, [4]Department of Physics and Astronomy, University of Western Ontario, London, Ontario, Canada, [5]Swedish Institute of Space Physics, Uppsala, Sweden

Abstract Little is currently known about the optical phenomenon known as Steve. The first scientific publication on the subject suggests that Steve is associated with an intense subauroral ion drift (SAID). However, additional inquiry is warranted as this suggested relationship as it is based on a single case study. Here we present eight occurrences of Steve with coincident or near-coincident measurements from the European Space Agency's Swarm satellites and show that Steve is consistently associated with SAID. When satellite observations coincident with Steve are compared to that of typical SAID, we find the SAID associated with Steve to have above average peak ion velocities and electron temperatures, as well as extremely low plasma densities.

1. Introduction

A new optical phenomenon has recently been brought to the attention of the space physics community by auroral photographers. Steve is observed as a latitudinally narrow, longitudinally extended purple band of light equatorward of the auroral oval. MacDonald et al. (2018) presented the first scientific report of Steve, and investigated the phenomenon simultaneously with a ground-based all-sky imager (ASI), photographs taken by citizen scientists, and in situ measurements from the European Space Agency's Swarm A satellite. These observations showed the optical signature of Steve to be roughly colocated with a subauroral ion drift (SAID). Typical of SAID, this event was located at the equatorward edge of the premidnight region 2 (R2) downward current system in the midlatitude density trough. MacDonald et al. (2018) also reported that the SAID associated with Steve was unusually intense. These initial results show Steve to be a subauroral phenomenon, and as it was measured within a region of weak downward field-aligned current (FAC), unlikely to be caused by precipitating electrons. This result was supported by Gallardo-Lacourt et al. (2018) who present particle measurements from Polar Orbiting Environmental Satellite coincident with an occurrence of Steve identified in ASI measurements. They reported an absence of precipitating charged particles coincident with the optical signature of Steve. In these previous studies, the name “Steve" was presented as the acronym for Strong Thermal Emission Velocity Enhancement. As the physical mechanisms responsible for this phenomenon have not yet been established, in this study we will simply refer to it as Steve.

What then is known about the physical mechanisms for Steve? Gallardo-Lacourt et al. (2018) suggested an ionospheric source for the optical phenomenon, as opposed to magnetospheric precipitating particles responsible for aurora. The results of MacDonald et al. (2018) suggested an association between SAID and Steve. Some characteristics of SAID may be responsible for Steve, or these two phenomena may share a generation mechanism. However, MacDonald et al. (2018) presented a single case study. Therefore, we cannot confidently state that Steve is consistently associated with SAID or that those SAID are unusually intense. In this study we present seven additional occurrences of Steve (as well as the event presented by MacDonald et al., 2018) identified in ASI measurements with near-coincident in situ measurements from the Swarm satellite mission. We show that in all cases, there is evidence of SAID associated with Steve. Furthermore, we determine that for the cases when Swarm satellites passed directly above Steve, they measured extreme plasma parameters relative to most SAID. These observations suggest that the case study presented by MacDonald et al. (2018) is representative of a consistent association between intense SAID and Steve.

SAID initially form near the poleward edge of the midlatitude density trough during geomagnetically active conditions (Spiro et al., 1978). SAID are associated with very little Pedersen current (compared to the auroral zone) and can have flows of several kilometers per second due to the low conductivity of the midlatitude trough. The accepted view of the trough during geomagnetically quiet conditions is that the combination of the dawn-dusk and the corotation electric fields results in a region of stagnation in darkness, allowing recombination to result in a region of relatively low plasma density, n_e (Brinton et al., 1978). The electron temperature, T_e, within the trough is typically anticorrelated with plasma density. This anticorrelation has often been described in terms of a relatively evenly distributed topside electron heat flux acting on regions with different plasma density. Regions of lower n_e have higher T_e as lower plasma densities result in greater thermal energy available per electron. During active conditions, the fast flows of SAID can further decrease the density in the trough through increased production of NO^+, which quickly dissociatively recombines (Schunk et al., 1976). Anderson et al. (1991) report significant NO^+ concentrations around 250-km altitude associated with SAID. See Moffett and Quegan (1983) for a more in-depth description of the midlatitude density trough. Richards et al. (2014) suggested an additional mechanism for generating the trough during geomagnetically active conditions. They presented observations of a summertime trough around 21 MLT that is difficult to explain through convection stagnation as most of the high-latitude region remains sunlit at this time. Richards et al. (2014) proposed that the observed trough was caused by plasma that had previously been corotating with the Earth in darkness before being drawn sunward by an expanding convection pattern.

Several optical signatures have been previously reported in the subauroral region. Pedersen et al. (2007) reported feint optical structures as far as 10° equatorward of the traditional auroral oval. This phenomena seem to be different from Steve as they are associated with kiloelectronvolt electron precipitation and are described as "highly structured." Stable auroral red (SAR) arcs are likely the subauroral optical phenomena that have been most thoroughly studied. They form in the midlatitude density trough when temperatures exceed 3500 K presumably by electron heat conduction from the magnetosphere that has been enhanced by interactions between the ring current and plasmaspheric electrons during geomagnetic storms (Fok et al., 1993; Thorne & Horne, 1992). At these temperatures there are sufficient high-energy electrons among the thermal population to excite SAR arcs (Cole, 1965; Kozyra et al., 1990). Foster et al. (1994) observed a SAR arc to be coincident with an ion drift of ~500 m/s in the midlatitude density trough during a geomagnetic storm. SAR arcs have a mean duration of 10 hr, have a typical latitudinal width of 500 km, and radiate in red at 630 nm (see ; Kozyra & Nagy, 1997, and references therein). Khalipov et al. (2001) suggested that some of the SAR arcs presented in the literature are connected to SAID and are not "classical" SAR arcs and reported weak (subvisual) optical signatures associated with SAID. Sazykin et al. (2002) presented a model description of this optical signature and found that like SAR arcs, hot thermal electrons colocated with SAID could contribute significantly to the observed optical signature. However, unlike SAR arcs, Sazykin et al. (2002) show that ion-neutral frictional heating could also significantly contribute to the observed optical emissions due to the large ion velocities associated with SAID. In this study we will present Swarm satellite measurements coincident with multiple occurrences of Steve to solidify the relationship between SAID and Steve and to provide in situ observations to constrain possible generation mechanisms of Steve.

2. Methodology

The optical measurements presented in this study are from the Time History of Events and Macroscale Interactions during Substorm (THEMIS) and the Redline Geospace Observatory (REGO) ASI arrays. The THEMIS ASIs are while light CCD imagers, each with a temporal resolution of 3 s and a spatial resolution of ~100 m near the zenith. For more information on the THEMIS ASI, see Donovan et al. (2006) and Mende et al. (2008). The REGO imagers are sensitive to wavelengths between ~628 and 632 nm, each with a temporal resolution of 3 s, and a spatial resolution of ~1.5 km near the zenith. For more information on the REGO ASI, see Liang et al. (2016) and Gillies et al. (2017). For this study Steve events were identified as a narrow band of emissions immediately equatorward of and separated from the auroral oval; many of these events are those presented by Gallardo-Lacourt et al. (2018). Using both the THEMIS ASI and REGO data sets, we identified 33 occurrences of Steve. Of these, 23 events were identified in THEMIS ASI observations from December 2007 to December 2015, and 10 events were identified in REGO ASI observations from November 2014 to October 2018. It should be noted that while a purple color is a defining feature of Steve when observed with the naked eye, many of the optical measurements in this study are made with REGO imagers (only sensitive to red light).

The Swarm satellites passed within 2 hr MLT of 8 of the 33 occurrences of Steve identified in optical measurements, providing in situ ionospheric measurements near Steve. The measurements from the satellites are well suited for the study of ionospheric subauroral phenomena. Their polar orbits precess through all magnetic local time every 4.5 months and the midlatitude density trough can often be identified at Swarm altitudes (between 450 and 500 km; Yizengaw & Moldwin, 2005). The Swarm satellites measure electric and magnetic fields, as well as electron density and temperature; see Jørgensen et al. (2008) and Knudsen et al. (2017) for more information on the Swarm instrument package. Plasma density and electron temperature measurements are from the Langmuir probe (LP) extended data set. Ion velocity, $\mathbf{v_i}$, measurements presented in this study are from the 16-Hz thermal ion imager cross-track data set. FAC measurements presented in this study are based on single-satellite magnetometer measurements and assume that the satellites are passing through infinite sheets of current. In this study we present measurements from all three Swarm satellites, which implies that the satellites are all calibrated to one another. While a direct intersatellite comparison has not been done for the Swarm satellites, scientific publications using multiple Swarm satellites (Archer et al., 2015; Goodwin et al., 2015; Spicher et al., 2015) as well as validation studies (Lomidze et al., 2017, 2019) all show the Swarm satellites to behave similarly to one another.

In order to directly compare ground-based optical to in situ satellite measurements, we mapped the geographic position of the Swarm satellites down to 230-km altitude, following International Geomagnetic Reference Field magnetic field lines. We did this using a fixed-step, leapfrog method described in Kouznetsov and Knudsen (2013). All coincident optical measurements in this study are from REGO, which we mapped to 230-km altitude. This is the typical altitude red line emissions are mapped to (Gillies et al., 2017). We identified the window of time that the magnetic footprint of the Swarm satellites spent colocated with the optical signature of Steve to estimate the location of Steve relative to measurements made by the Swarm satellites. A sample ASI image with satellite orbit and estimated location of Steve overlaid is provided as supporting information.

To provide a standard to which these Steve events can be compared, we identified SAID events in Swarm measurements as velocity peaks exceeding 500 m/s separated spatially from the auroral convection flows and colocated with the midlatitude density trough. This is a typical operational definition of SAID in the absence of particle measurements (Spiro et al., 1978). Between 11 December 2013 (earliest electric field measurements from the mission) and 31 December 2014, 122 SAID events were identified in Swarm A measurements. This time period was selected as it samples all MLT roughly equally, all seasons equally, and there are few gaps in Swarm cross-track plasma flow measurements. These events are ideal for comparison with measurements of Steve as they were made by a single instrument at similar altitudes. A list of their times is available in the supporting information.

In this study we compare SAID and Steve events by the plasma parameters measurements provided by the Swarm satellites. We compare the extrema of most plasma parameters; namely, maximum v_i, maximum T_e, and minimum n_e. To characterize the modest localized enhancement in downward FAC associated with SAID (He et al., 2016), we integrated FAC over ~30 km surrounding each SAID/Steve event, to estimate the total FAC enhancement of each event.

3. Results

3.1. Steve Measurements With Swarm

At the time of this study 33 occurrences of Steve have been identified in scientific optical measurements. Of those events, a Swarm satellite passed directly above or near Steve on eight occasions. Figure 1 shows the plasma parameters measured by the Swarm satellites for all eight events, plotted in altitude-adjusted corrected geomagnetic latitude (MLat). Each crossing is centered on the position at which the maximum electron temperature was measured within the midlatitude density trough. Event c corresponds to the occurrence of Steve presented by MacDonald et al. (2018). The LP measurements presented in this study are superficially different than those presented by MacDonald et al. (2018), as they were processed by a more recent algorithm. In cases where Swarm passed directly above Steve within the field of view of an ASI, the approximate location of Steve is shown as a gray-shaded box in Figure 1. The optical signature of Steve is very faint in most cases, and these shaded areas only roughly mark the boundaries of Steve and are as such significantly wider than the average full width at half maximum of ~20 km reported by Gallardo-Lacourt et al. (2018). For event e, at the time that Swarm C passed through the field of view of the ASI, its orbit was roughly 0.8 h west of the westmost extent of Steve. Steve then expanded eastward along the equatorward

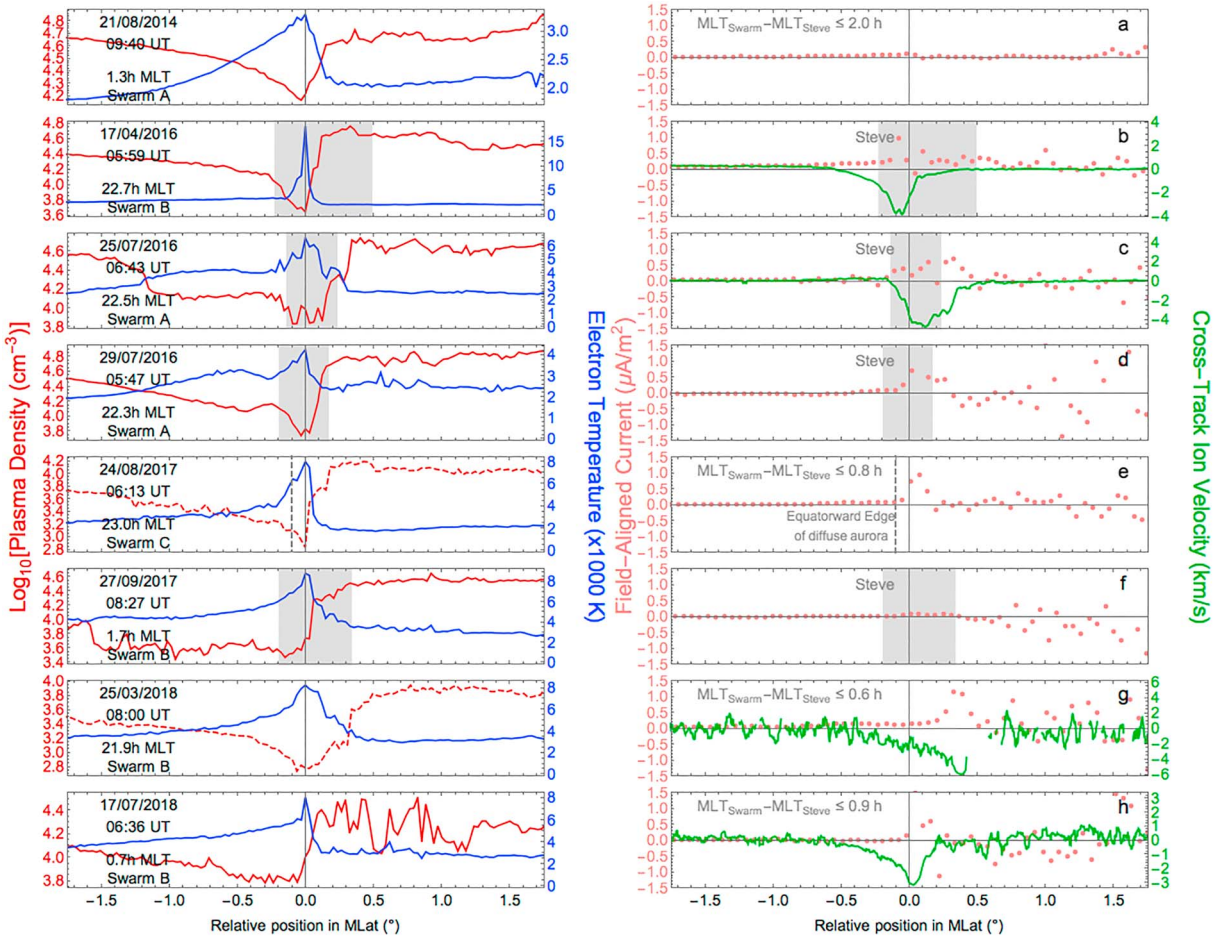

Figure 1. Plasma density and electron temperature (left panels) and field-aligned current and ion velocity (right panels) measured by Swarm satellites passing near/through Steve events that had been identified in all-sky imager measurements for eight events. Plasma density is shown in red with solid lines estimated from Langmuir probed ion current and dashed lines estimated from electron current. Electron temperature is shown in blue. Field-aligned current is shown in pink. Cross-track ion velocity is shown in green. Location of Steve along the satellite track is shaded in gray. The equatorward edge of the diffuse aurora is marked with a dashed gray line for the event e, from 24 August 2017. Steve = Strong Thermal Emission Velocity Enhancement.

edge of the diffuse aurora, reaching the MLT of the Swarm orbit only 2 min after the satellite crossed. A gray dashed line for event e in Figure 1 shows the optical boundary of the diffuse aurora (where Steve forms 2 min after the Swarm crossing). In events a, g, and h, conditions were cloudy directly beneath the Swarm satellites, and so Steve was identified in adjacent ASI. In these cases the MLT difference between Swarm and nearest observed point of Steve (seen at the edge of the closest ASI) is listed in Figure 1. This represents the maximum possible distance between Swarm and Steve as we do not know how far Steve extends beyond the field of view of the cameras and can span over 2,000 km in latitude (Gallardo-Lacourt et al., 2018). At the latitudes of the observations presented in Figure 1 near the surface of the Earth, 1 hr of MLT corresponds to roughly 800 km in longitudinal separation. It should be noted that ion velocity measurements are only available in four cases, as the Swarm electric field instrument (EFI) was not operating for the other events. Also, for the Swarm mission n_e is typically derived from LP ion current (measured at negative probe bias). Plasma density is often derived from ion rather than electron saturation current, as it is independent of electron temperature. However, in a few cases this n_e reached negative values, possibly because of inaccurately calibrated electronic offsets. In those cases, n_e is instead estimated from LP electron current and is shown as a dashed red line (rather than a solid one) in Figure 1.

For all cases in Figure 1, a clear midlatitude density trough is observed in Swarm measurements, with a peak in T_e (shown in blue) roughly colocated with the minimum in n_e (shown in red). The FAC (shown in pink) when crossing the point of maximum T_e for all cases was either positive, indicating a downward FAC, or near zero. Narrow channels of enhanced westward ion velocity (shown in green) were also observed roughly

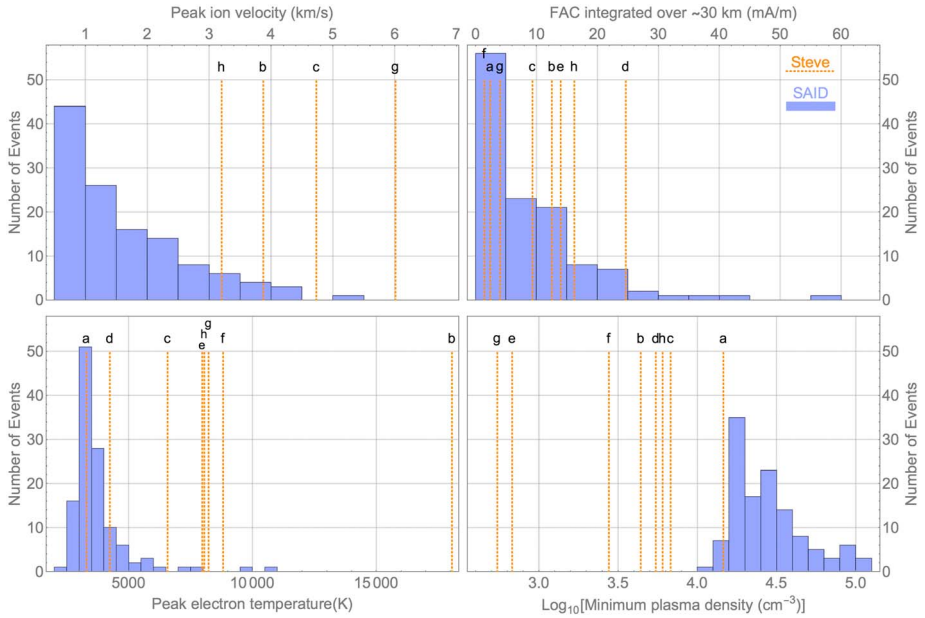

Figure 2. Histograms of (top left) plasma peak ion velocity, (top right) field-aligned current integrated over 30 km, (bottom left) peak electron temperature, and (bottom right) minimum plasma density measured by the Swarm A satellite coincident with 122 SAID events identified between 11 December 2013 and 31 December 2014. Plasma parameters measured coincident with Steve events shown as red dashed lines on histograms. SAID = subauroral ion drift; Steve = Strong Thermal Emission Velocity Enhancement.

colocated with the minimum n_e for all cases in which the Swarm EFI was operating. The EFI was turned on shortly after event a, and a 800-m/s flow channel was observed coincident with the midlatitude density trough on the subsequent orbit (1.5 hr later). It should be noted that because there are no v_i measurements available for four of the events in Figure 1, they do not meet the criteria used in this study to identify SAID. However, in all cases the available Swarm measurements presented in Figure 1 match typical past SAID observations from ~500 km altitude (Anderson et al., 1991; Archer & Knudsen, 2018; Spiro et al., 1979), and are all roughly colocated with occurrences of Steve. We also note that while SAID are reported between 16 and 2 hr MLT with the highest occurrence probability density around 22 MLT (He et al., 2014; Spiro et al., 1979), all Steve events presented so far have been between 22 and 2 MLT.

The observations shown in Figure 1 are qualitatively very similar to those presented by Foster et al. (1994) coincident with a SAR arc. The peak flow enhancement observed by Foster et al. (1994) was ~500 m/s and filled the midlatitude density trough and was accompanied by a peak electron temperature of ~4000 K. Prölss (2006) showed subauroral T_e enhancements of about 3000 K using the LP on the DE-2 satellite. Contrasting these observations, the narrower flow channels situated at the poleward edge of the trough in Figure 1 have peak velocities of several kilometers per second and are colocated with peak electron temperatures ranging from 4000 K to over 10000 K. To provide context for the magnitude of these values, in the next section we establish what is typically observed by the Swarm satellites when crossing SAID.

3.2. Comparing Steve to Typical SAID

We identified 122 SAID events exceeding 500 m/s in peak v_i in Swarm A measurements, which we use to represent typical plasma parameters for SAID when measured from Swarm altitudes. Figure 2 shows histograms of the peak v_i, peak T_e, minimum n_e, and integrated FAC (over ~30 km) for all 122 events. Superposed on these histograms are orange vertical dashed lines, representing the plasma parameters measured by the Swarm satellites that passed through (or near to) Steve. The measurements associated with Steve events have been labeled with lower case letters matching the labels in Figure 1.

Figure 2 shows the majority of SAID to have a FAC integrated over 30 km of less than 10 mA/m. The integrated FAC for the Steve events do not clearly fit nor do they clearly deviate from the distribution established by SAID. The Steve events do, however, clearly deviate from typical SAID in v_i, T_e, and n_e. SAID ion velocities in Figure 2 are most frequently less than 500 m/s, with a median velocity of ≈1.3 km/s. The SAID coincident with Steve events shown in Figure 2 have ion velocities exceeding 3 km/s and are all in the top 5th

percentile relative to typical SAID. Similarly, the peak T_e of six of the eight Steve events in Figure 2 are in the top 3% of peak T_e of SAID. Most striking perhaps is n_e, where the minimum n_e for all Steve events except one are less than any measured for typical SAID. It should be noted that satellite observations for event a, which has relatively low v_i and T_e, as well as relatively high n_e, were taken the farthest from the ASI field of view detecting Steve among events presented in this study. This analysis is limited by the small number of observations of Steve. However, a clear pattern emerges in which Steve is consistently associated with intense SAID with unusually large v_i, high T_e, and extremely low n_e.

4. Discussion and Conclusion

The first scientific publication on Steve (MacDonald et al., 2018) showed the phenomenon to be colocated with an intense SAID. This association between Steve and SAID was based on a single event. We have expanded on the work of MacDonald et al. (2018) by identifying eight occurrences of Steve with coincident or near-coincident Swarm satellite measurements. In all cases, Steve is observed roughly colocated with the minimum n_e and corresponding maximum T_e of the midlatitude density trough. We observe a narrow westward flow channel, consistent with a SAID, for all cases that Swarm ion velocity measurements are available. We found no counter examples to this trend. In other words, for every Swarm crossing near Steve, measurements consistent with SAID were observed. Additionally, these events are intense relative to the average SAID with large v_i, high T_e, and low n_e. How then, does this inform us on the generation mechanism of Steve?

It is clear from REGO observations that Steve radiates in red frequencies. The T_e and v_i measured coincident with Steve are both significantly higher than the values modeled by Sazykin et al. (2002), suggesting that electron impact and ion-neutral frictional heating may both contribute to the red emissions of Steve. The spectral properties of Steve are currently unknown, but a purple glow appears to be a persistent feature. The purple observed in traditional aurora is caused by the deexcitation of N_2^+. However, the optical signature of Steve appears to originate around 230 km, significantly higher altitudes than we expect N_2^+ emissions (Måseide, 1967). The purple appearance of Steve could be due to either violet emissions or a mixture of red with other emissions such as the green line and/or blue line emissions at 557.7 and 427.8 nm with the minimum excitation energies of about 4.2 and 18.8 eV, respectively. If electron impact is responsible for such emissions within Steve, a population of suprathermal electrons is required significantly beyond that of the Maxwellian tail of the heated thermal electrons in order that the brightness of these emissions be comparable with the red line emission. The presence of such suprathermal electrons in SAID events has been reported from Defense Meteorological Satellite Program (DMSP) observations in the topside ionosphere and Combined Release and Radiation Effects Satellite (CRRES), Time History of Events and Macroscale Interactions during Substorms (THEMIS), Van Allen Probes (VAP), and Polar observations in the conjugate plasmasphere (e.g., Mishin, 2013; Mishin et al., 2017).

The extrema in T_e and v_i associated with SAID are often roughly colocated; they are not exactly colocated. This significant distinction is discussed by Moffett et al. (1998), and in this study is most evident for Case g in Figure 1. Unfortunately, the in situ and ground-based observations for Case g were not perfectly coincident, as they may have otherwise shed light on the relative importance of elevated T_e and v_i on the formation of Steve. On a similar note, we must keep in mind that the in situ observations from the Swarm satellites are well above the emission altitudes of Steve. While the latitudinal profiles of v_i presumably map down magnetic field lines, the latitudinal profiles of T_e and n_e will vary with altitude. As such, directly comparing the latitudinal profiles of optical emission, T_e, and v_i at Swarm altitudes will not perfectly reflect what is occuring at Steve emission altitudes.

Several key observations of Steve are still required before a proper simulation of the phenomenon can be carried out. Specifically, the spectral characteristics Steve and altitude range at which it occurs has yet to be determined, and would greatly constrain models of Steve. Regardless of the specific mechanisms responsible for Steve, the observations presented in this study suggest Steve to be the optical signature of exceptionally intense SAID.

Acknowledgments
This study is based on Level 1B and Level 2 Swarm data available at https://earth.esa.int/web/guest/swarm/ data access. Swarm is a project of the European Space Agency. The entire LP density estimates using the electron current are not yet included in the extended LP data set but will be in the next version. The LP currents and n_e estimates used in this work are made available at https://www.space.irfu.se/steve/. Login and password are provided by S. Buchert upon request. William Archer was supported by grants from the European Space Agency and the Natural Sciences and Engineering Council of Canada. The ASI data used in this study were produced with funding from the Canadian Space Agency and National Science Foundation. THEMIS ASI data can be viewed via the University of Calgary data portal located at http://data-portal.phys.ucalgary.ca/. We would like to thank Alexei Kouznetsov for his software used to trace IGRF12 magnetic field lines.

References

Anderson, P. C., Heelis, R. A., & Hanson, W. B. (1991). The ionospheric signatures of rapid subauroral ion drifts. *Journal of Geophysical Research*, *96*(90), 5785–5792. https://doi.org/10.1029/90JA02651

Archer, W. E., & Knudsen, D. J. (2018). Distinguishing subauroral ion drifts from Birkeland current boundary flows. *Journal of Geophysical Research: Space Physics*, *2016*, 819–826. https://doi.org/10.1002/2017JA024577

Archer, W. E., Knudsen, D. J., Burchill, J. K., Patrick, M. R., & St.-Maurice, J.-P. (2015). Anisotropic core ion temperatures associated with strong zonal flows and upflows. *Geophysical Research Letters*, *42*, 981–986. https://doi.org/10.1002/2014GL062695

Brinton, H. C., Grebowsky, J. M., & Brace, L. H. (1978). The high-latitude winter *F* region at 300 km: Thermal plasma observations from AE-C. *Journal of Geophysical Research*, *83*(A10), 4767–4776. https://doi.org/10.1029/JA083iA10p04767

Cole, K. D. (1965). Stable auroral red arcs, sinks for energy of Dst main phase. *Journal of Geophysical Research*, *70*(7), 1689–1706. https://doi.org/10.1029/JZ070i007p01689

Donovan, E., Mende, S., Jackel, B., Frey, H., Syrjäsuo, M., Voronkov, I., et al. (2006). The THEMIS all-sky imaging array-system design and initial results from the prototype imager. *Journal of Atmospheric and Solar-Terrestrial Physics*, *68*(13), 1472–1487. https://doi.org/10.1016/j.jastp.2005.03.027

Fok, M.-C., Kozyra, J. U., Nagy, A. F., Rasmussen, C. E., & Khazanov, G. V. (1993). Decay of equatorial ring current ions and associated aeronomical consequences. *Journal of Geophysical Research*, *98*(1), 19,381–19,393.

Foster, J. C., Buonsanto, M. J., Mendillo, M., Nottingham, D., Rich, F. J., & Denig, W. (1994). Coordinated stable auroral red arc observations: Relationship to plasma convection. *Journal of Geophysical Research*, *99*(A6), 11,429–11,439. https://doi.org/10.1029/93JA03140

Gallardo-Lacourt, B., Liang, J., Nishimura, Y., & Donovan, E. (2018). On the origin of STEVE: Particle precipitation or ionospheric skyglow? *Geophysical Research Letters*, *45*, 7968–7973. https://doi.org/10.1029/2018GL078509

Gallardo-Lacourt, B., Nishimura, Y., Donovan, E., Gillies, D. M., Perry, G. W., Archer, W. E., et al. (2018). A statistical analysis of STEVE. *Journal of Geophysical Research: Space Physics*, *123*, 9893–9905. https://doi.org/10.1029/2018JA025368

Gillies, D. M., Knudsen, D., Donovan, E., Jackel, B., Gillies, R., & Spanswick, E. (2017). Identifying the 630 nm auroral arc emission height: A comparison of the triangulation, FAC profile, and electron density methods. *Journal of Geophysical Research: Space Physics*, *122*, 8181–8197. https://doi.org/10.1002/2016JA023758

Goodwin, L. V., Iserhienrhien, B., Miles, D. M., Patra, S., Meeren, C. V. D., Buchert, S. C., et al. (2015). Swarm in situ observations of *F* region polar cap patches created by cusp precipitation. *Geophysical Research Letters*, *42*, 996–1003. https://doi.org/10.1002/2014GL062610. High-resolution.

He, F., Zhang, X. X., & Chen, B. (2014). Solar cycle, seasonal, and diurnal variations of subauroral ion drifts: Statistical results. *Journal of Geophysical Research: Space Physics*, *120*, 5009–5021. https://doi.org/10.1002/2015JA021023. Received.

He, F., Zhang, X. X., Wang, W., & Chen, B. (2016). Double-peak subauroral ion drifts (DSAIDs). *Geophysical Research Letters*, *43*, 5554–5562. https://doi.org/10.1002/2016GL069133

Jørgensen, J. L., Friis-Christensen, E., Brauer, P., Primdahl, F., Jørgensen, P. S., Allin, T. H., & Denver, T. (2008). The Swarm magnetometry package. In *Small satellites for earth observation* (pp. 143–151). Berlin: Springer.

Khalipov, V. L., Galperin, Y. I., Stepanov, A. E., & Shestakova, L. V. (2001). Formation of a polarization jet during the expansion phase of a substorm : Results of ground-based measurements. *Cosmic Research*, *39*(3), 244–253.

Knudsen, D. J., Burchill, J. K., Buchert, S. C., Eriksson, A., Gill, R., Wahlund, J.-E., et al. (2017). Thermal ion imagers and Langmuir probes in the Swarm electric field instruments. *Journal of Geophysical Research: Space Physics*, *122*, 2655–2673. https://doi.org/10.1002/2016JA022571

Kouznetsov, A., & Knudsen, D. J. (2013). Forward mapping of solar energetic proton distributions through the geomagnetic field. *Journal of Geophysical Research: Space Physics*, *118*, 4724–4738. https://doi.org/10.1002/jgra.50400

Kozyra, J. U., & Nagy, A. F. (1997). High-altitude energy source(s) for stable auroral red arcs. *Reviews of Geophysics*, *25*(96), 155–190.

Kozyra, J. U., Valladares, C. E., Carlson, H. C., Buonsanto, M. J., & Slater, D. W. (1990). Study of the seasonal and solar cycle variations of stable aurora red arcs. *Journal of Geophysical Research*, *95*(A8), 12,219–12,234.

Liang, J., Donovan, E., Jackel, B., Spanswick, E., & Gillies, D. M. (2016). On the 630 nm red-line pulsating aurora: Red-line Emission Geospace Observatory observations and model simulations. *Journal of Geophysical Research: Space Physics*, *121*, 7988–8012. https://doi.org/10.1002/2016JA022901. Received.

Lomidze, L., Burchill, J. K., Knudsen, D. J., Kouznetsov, A., & Weimer, D. R. (2019). Validity study of the Swarm horizontal cross—Ion drift velocities in the high-latitude ionosphere. *Earth and Space Science*, *6*, 411–432. https://doi.org/10.1029/2018EA000546

Lomidze, L., Knudsen, D. J., Burchill, J. K., Kouznetsov, A., & Buchert, S. C. (2017). Calibration and Validation of Swarm plasma densities and electron temperatures using ground-based radars and satellite radio occulation measurements. *Radio Science*, *53*, 15–36. https://doi.org/10.1002/2017RS006415

Måseide, K. (1967). Rocket measurements of the volume profile for auroral glow. *Planetary and Space Science*, *15*, 899–905.

MacDonald, E. A., Donovan, E., Nishimura, Y., Case, N. A., Gillies, D. M., Gallardo-lacourt, B., et al. (2018). New science in plain sight: Citizen scientists lead to the discovery of optical structure in the upper atmosphere. *Science Advances*, *4*(March), 16–21. https://doi.org/10.1126/sciadv.aaq0030

Mende, S. B., Harris, S. E., Frey, H. U., Angelopoulos, V., Russell, C. T., Donovan, E., et al. (2008). The THEMIS array of ground-based observatories for the study of auroral substorms. *Space Science Reviews*, *141*(1-4), 357–387. https://doi.org/10.1007/s11214-008-9380-x

Mishin, E. V. (2013). Interaction of substorm injections with the subauroral geospace : 1. Multispacecraft observations of SAID. *Journal of Geophysical Research: Space Physics*, *118*, 5782–5796. https://doi.org/10.1002/jgra.50548

Mishin, E. V., Nishimura, Y., & Foster, J. (2017). SAPS/SAID revisited: A causal relation to the substorm current wedge. *Journal of Geophysical Research: Space Physics*, *122*, 8516–8535. https://doi.org/10.1002/2017JA024263

Moffett, R. J., Ennis, A. E., Bailey, G. J., Heelis, R. A., & Brace, L. H. (1998). Electron temperatures during rapid subauroral ion drift events. *Annales Geophysicae*, *16*(4), 450. https://doi.org/10.1007/s005850050615

Moffett, R. J., & Quegan, S. (1983). The mid-latitude trough in the electron concentration of the ionospheric *F*-layer: A review of observations and modelling. *Journal of Atmospheric and Terrestrial Physics*, *45*(5), 315–343. https://doi.org/10.1016/S0021-9169(83)80038-5

Pedersen, T., Mishin, E., & Oksavik, K. (2007). Observations of structured optical emissions and particle precipitation equatorward of the traditional auroral oval. *Journal of Geophysical Research*, *112*, 1–14. https://doi.org/10.1029/2007JA012299

Prölss, G. W. (2006). Subauroral electron temperature enhancement in the nighttime ionosphere. *Annales Geophysicae*, *24*, 1871–1885.

Richards, P. G., Nicolls, M. J., St.-Maurice, J. P., Goodwin, L., & Ruohoniemi, J. M. (2014). Investigation of sudden electron density depletions observed in the dusk sector by the Poker Flat, Alaska incoherent scatter radar in summer. *Journal of Geophysical Research A: Space Physics*, *119*, 10,608–10,620. https://doi.org/10.1002/2014JA020541

Sazykin, S., Fejer, B. G., Galperin, Y. I., Zinin, L. V., Grigoriev, S. A., & Mendillo, M. (2002). Polarization jet events and excitation of weak SAR arcs. *Geophysical Research Letters*, *29*(12), 1586. https://doi.org/10.1029/2001GL014388

Schunk, R. W., Banks, P. M., & Raitt, W. J. (1976). Effects of electric fields and other processes upon the nighttime high-latitude *F* layer. *Journal of Geophysical Research*, *81*(19), 3271–3282. https://doi.org/10.1029/JA081i019p03271

Spicher, A., Cameron, T., Grono, E. M., Yakymenko, K. N., Buchert, S. C., Clausen, L. B. N., et al. (2015). Observation of polar cap patches and calculation of gradient drift instability growth times: A Swarm case study. *Geophysical Research Letters*, *42*, 201–206. https://doi.org/10.1002/2014GL062590

Spiro, R. W., Heelis, R. A., & Hanson, W. B. (1978). Ion convection and the formation of the mid-latitude *F* region ionization trough. *Journal of Geophysical Research*, *83*, 4255–4264. https://doi.org/10.1029/JA083iA09p04255

Spiro, R. W., Heelis, R. A., & Hanson, W. B. (1979). Rapid subauroral ion drifts observed by atmosphere explorer C. *Geophysical Research Letters*, *6*(8), 657–660. https://doi.org/10.1029/GL006i008p00657

Thorne, R. M., & Horne, R. B. (1992). The contribution of ion-cyclotron waves to electron heating and SAR-arc excitation near the storm-time plasmapause. *Geophysical Research Letters*, *19*(4), 417–420.

Yizengaw, E., & Moldwin, M. B. (2005). The altitude extension of the mid-latitude trough and its correlation with plasmapause position. *Geophysical Research Letters*, *32*, L09105. https://doi.org/10.1029/2005GL022854

Appendix B

Geophysical Research Letters

RESEARCH LETTER
10.1029/2019GL084473

The Vertical Distribution of the Optical Emissions of a Steve and Picket Fence Event

W. E. Archer[1], J.-P. St.- Maurice[1,2], B. Gallardo-Lacourt[3], G. W. Perry[4], C. M. Cully[5], E. Donovan[5], D. M. Gillies[5], R. Downie[6], J. Smith[6], and D. Eurich[6]

[1]Department of Physics and Engineering Physics, University of Saskatchewan, Saskatoon, Saskatchewan, Canada, [2]Department of Physics and Astronomy, University of Western Ontario, London, Ontario, Canada, [3]NASA/GSFC, Greenbelt, MD, USA, [4]Center for Solar-Terrestrial Research, New Jersey Institute of Technology, Newark, NJ, USA, [5]Department of Physics and Astronomy, University of Calgary, Calgary, Alberta, Canada, [6]Alberta Aurora Chasers, Calgary, Alberta, Canada

Key Points:
- The optical emissions of Steve range from 130 to 270 km in altitude
- The optical emissions of the green Picket Fence range from 95 to 150 km in altitude
- Steve and the Picket Fence extend vertically along similar magnetic field lines

Supporting Information:
- Supporting Information S1

Correspondence to:
W. E. Archer,
wea784@usask.ca

Citation:
Archer, W. E., St.-Maurice, J.-P., Gallardo-Lacourt, B., Perry, G. W., Cully, C. M., & Donovan, E. et al. (2019). The vertical distribution of the optical emissions of a Steve and Picket Fence event. *Geophysical Research Letters*, *46*, 10,719–10,725. https://doi.org/10.1029/2019GL084473

Received 8 JUL 2019
Accepted 29 AUG 2019
Accepted article online 3 SEP 2019
Published online 11 OCT 2019

Abstract So-called "Steve" subauroral purple emissions have recently been uncovered by auroral photographers and have rapidly become an intense subject of debate as to their origin. In some events, nearby periodic green emissions have also been uncovered and given the name "picket fence," owing to their appearance. The present paper advances our understanding of these phenomena by narrowing down the altitude extent of the Steve and picket fence emissions. Our determination is based on the event of 16 September 2017, which was simultaneously observed from two vantage points, allowing for a determination of the height range of Steve and picket fence through triangulation. We show that the picket fence extend between 95- and 150-km altitude and is aligned with the geomagnetic field, while the Steve altitude spread is between 130 and 270 km. We also show the two phenomena to be on nearby or perhaps the same magnetic field lines.

1. Introduction

The scientific community has recently reported on a nighttime optical phenomenon called Steve. Steve is described as a purple band of light observed equatorward of aurora, spanning only tens of kilometers in latitude but thousands of kilometers in longitude (Gallardo-Lacourt, Nishimura, et al., 2018). Archer et al. (2019) were able to find eight occurrences of Steve with near-coincident satellite measurements, and they show Steve to be consistently associated with intense subauroral ion drifts (SAID). The notion of Steve as an optical signature of SAID was put forward by MacDonald et al. (2018). Typical of SAID, these events were near the ionospheric projection of the plasmapause, with either near-zero or downward field-aligned current, which suggests that Steve is not caused by precipitating electrons. Particle measurements from the Polar Operational Environmental Satellites coincident with an occurrence of Steve shows there is insufficient particle precipitation to cause the optical signature of the phenomenon (Gallardo-Lacourt, Liang, et al., 2018). These studies suggest that Steve may be related to the plasma heating present in very intense SAID.

Steve is at times accompanied by green bands of light called the "picket fence." It is currently unknown if these two phenomena are causally linked. While Steve has been reported on several occasions in the absences of the picket fence, the picket fence has not yet been reported in isolation. Nishimura et al. (2019) presented measurements from the Defense Meteorological Satellite Program coincident with two different Steve events, one with picket fence and one without. They report a region of kiloelectron volts precipitating particles roughly coincident with the event including a picket fence, detached from the auroral oval. Based on these observations, Nishimura et al. (2019) suggest that while plasma heating may contribute to Steve, the picket fence seems to be caused by precipitating electrons.

Recent spectral measurements of the picket fence presented by Gillies et al. (2019) are also consistent with the phenomena being caused by precipitating electrons, as they show the picket fence to be dominated by OI 557.7-nm emissions. Gillies et al. (2019) also show that the spectral observations of Steve have two major contributing components: OI red-line emissions and a continuous spectral enhancement spanning approximately 400–730 nm. The red emissions could be caused by soft electron precipitation, except for the fact that, as previously stated, Steve does not appear to be coincident with precipitating particles. Alternatively, red emissions could result from the recombination of molecular oxygen as occurs in polar-cap patches

(Weber et al., 1984; Weber et al., 1986). Another possibility would be impact from hot thermal electron as occurs in stable red arcs (Cole, 1965; Kozyra et al., 1990). However, none of these mechanisms explain the purple appearance of Steve which, based on the work of Gillies et al. (2019), is due to a continuum visual spectrum. In many of these previous studies, the name "Steve" was presented as the acronym for Strong Thermal Emission Velocity Enhancement. As the physical mechanisms responsible for this phenomenon have not yet been established, in this study we will simply refer to it as Steve.

In order to further constrain the physical mechanisms that could be responsible for Steve and the picket fence, we have sought to determine the altitude range of the phenomena. Altitude estimates of Steve in previous studies (Archer et al., 2019; MacDonald et al., 2018) have been based on the presence of the atomic oxygen red-line emissions inside Steve, resulting in estimates around 230 km, as is typical for red-line emissions (Gillies et al., 2017). In the present study we have converged on one occurrence of the Steve and picket fence phenomena that took place from approximately 5–6 UT on 16 September 2017. Although no scientific ground-based optical measurements were taken of this event due to its location (south or west of the field-of-view of all-sky cameras), dozens of amateur auroral photographers captured Steve from western Alberta and eastern British Columbia. By comparing two simultaneous observations that were taken hundreds of kilometers apart in the north-south direction, we have narrowed down the altitude ranges and latitude of the two phenomena. We have also found that the observations are consistent with Steve and the picket fence being essentially on the same magnetic field lines.

2. Methodology

In order to interpret photographic observations of Steve, we first had to establish a coordinate system within each photograph. To do so, we relied on the background star field in each photograph. With the location and time of each photograph in hand, the azimuth and elevation angle of any given star in the night sky could be determined. From that information, we could in turn determine the exact angular position of the boundaries of the Steve and picket fence structures.

Most photographs of Steve are taken with a 20-s integration period. As a result, even stars with apparent magnitudes greater than 8 are clearly visible (the faintest stars visible by the unaided human eye have apparent magnitudes around 6.5). We identified stars using the "SkySafari" (2019) application and tabulated their azimuths and elevations from the "StarData" function available in Mathematica (2017). We could not establish a linear coordinate system over an entire image because the field of view of cameras is not flat. We defined the boundary of optical features by their brightness, the edge of the features being 50% of the peak emission intensity. The upper boundary of the picket fence cannot be identified with this boundary definition because the background (Steve) is too bright. For the upper boundaries of the picket fence, we instead qualitatively identified the region where the green of the picket fence transitioned into the white of Steve. We then identified stars angularly colocated with boundaries of optical features in order to directly measure the angular location of those optical features. Two examples of this are shown in Figure 1. Stars angularly colocated with the edge of Steve are marked with empty squares and triangles, while those colocated with the end of a picket fence are marked with filled squares and triangles. Squares mark the top or southern boundary of optical features (depending on the observers perspective), while triangles mark the bottom or northern boundary. Once we identified the angular positions of interest, we mapped them out into geodetic space using the aer2geodetic submodule within the pymap3d module for python (Hirsch, 2016).

The photograph in Figure 1a was taken by Robert Downie, who we will call Observer 1 (O1), at approximately 05:53:14 UT looking south from the campground near Berg Lake (53.1534° N, 119.1538° W, 1,680-m altitude). O1 took 109 photographs of Steve between 05:00 and 06:05 UT. This large number of photographs made it an ideal data set for comparison with photographs from other observers as it is likely that a temporally coincident photograph was taken. O1 was roughly 250 km north of Steve, so that, ideally, to minimize uncertainty in triangulation, a second observer should be located directly beneath Steve. One such photograph was obtained and is shown in Figure 1b. It was taken by Janis Smith (O2) from the shores of Shushwap Lake (50.9666° N, 119.3541° W, 530-m altitude). The location of O1, O2, and a third photographer named Dale Eurich (O3) are shown in Figure 1c along with the rough location of a portion of Steve accessed by the photographs and which has been shaded purple in Figure 1c.

To verify the time stamp of O1's photographs, we identified a star angularly colocated with the eastern peak of Mount Robson (53.1155° N, 119.1688° W, 3,400-m altitude). The star HD 206739 is highlighted in red

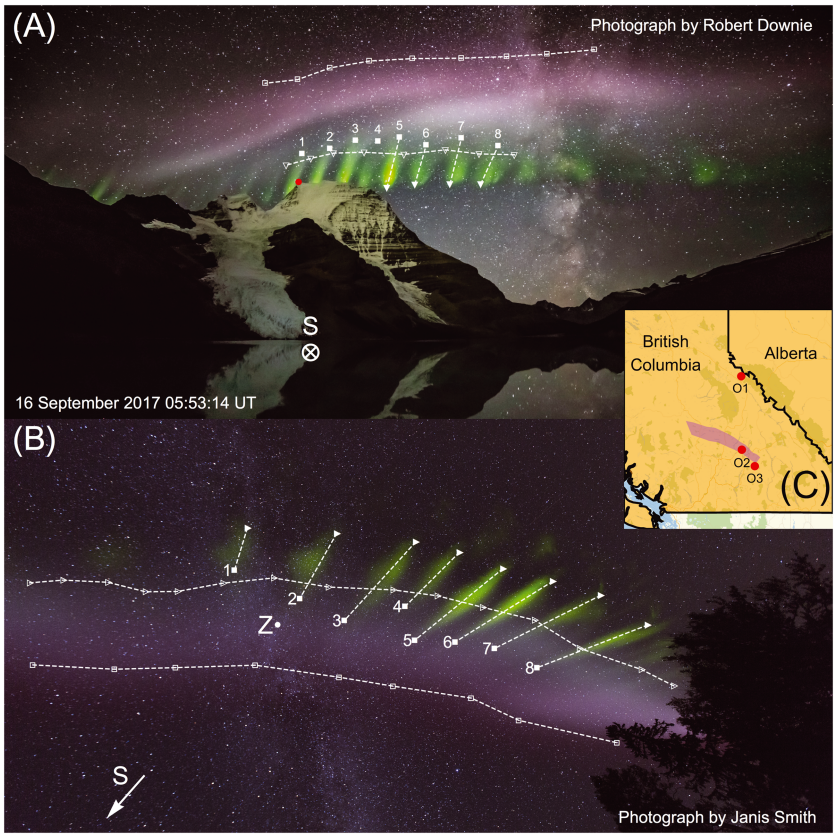

Figure 1. (a) Photograph of Steve taken around 05:53 UT on 16 September 2017 by Robert Downie (O1). The southward direction is labeled with S. Stars angularly colocated with the top and bottom edge Steve are marked with empty squares and triangles, respectively. Stars angularly colocated with the top and bottom of the picket fences are marked with filled squares and triangles, respectively. The star HD 206739, which is angularly colocated with the eastern edge of the top of Mount Robson, is marked with a red dot. (b) Photograph of Steve taken around 05:53 UT on 16 September 2017 by Janis Smith (O2). The southward and zenith directions are labeled with S and Z, respectively. Stars angularly colocated with the southern and northern edges of Steve are marked with empty squares and triangles, respectively. Stars angularly colocated with the southern and northern edges of the picket fences are marked with filled squares and triangles, respectively. In both (a) and (b), the picket fence structures are enumerated for reference. (c) The position of O1, O2, and Dale Eurich (O3) are shown along with a rough estimate of the location of a portion Steve.

in Figure 1a and had a position of 178.3° azimuth, 25.1° elevation from O1's position at the recorded time of the photograph. This is within 1° of the expected location of the eastern peak of Mount Robson (178.2° azimuth, 24.3° elevation) and confirms O1's time stamp to be accurate to within 1 min. The time stamps of O2's photographs could not be relied on. We therefore identified a photograph by O1 that was most likely to be coincident with O2's photograph by comparing the optical structures recorded by the two observers. O2 took four photographs of Steve over a period of 28 min. By comparing the temporal evolution of Steve reported by O2 and O1, we determined that the photograph shown in Figure 1b was taken between 05:50 and 05:55 UT. We then further refined our time determination by mapping out the angular position of the picket fence structure reported by the two observers. The latter was steadily moving westward (at between 200 and 300 m/s), and we identified the O1 photograph shown in Figure 1a to be the image most likely to coincide with O2's photograph. During this period of time, O1 took a photograph every 20 s. As such, we know the relative timing of O1 and O2's photographs to within 20 s. Assuming a time stamp of 05:53:14 UT for O2's photograph, her picket fence observations mapped into geodetic coordinates pass within 2 km horizontally of O1's photograph. Also note that both observers reported the fourth picket when counting east to west to be shorter than either of its neighbors.

Having identified the most likely time at which O2's photograph was taken, we estimated the altitude of Steve and the picket fence based on the photographs shown in Figure 1. For the picket fence, this was done by mapping out the altitude and azimuth of the top and bottom of each green picket from both perspectives

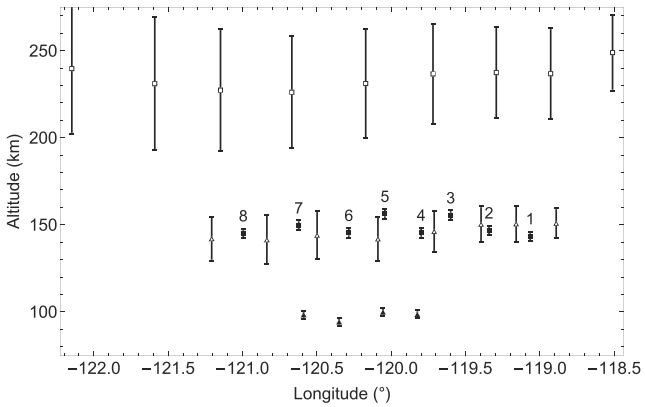

Figure 2. Most likely altitudes and longitudes of the boundaries of Steve and the picket fence identified in Figure 1a. The top and bottom of Steve are marked with empty squares and triangles, respectively. The top and bottom of the picket fence are marked with filled squares and triangles, respectively. The picket fence structures are enumerated in the same fashion as in Figure 1a for reference.

and identifying the point at which the two rays (nearly) intersected. For example, the top of the westmost picket that is marked with an filled square in Figure 1 is angularly coincident with the star HD 185762 from O1's perspective, which was at 214.85° azimuth and 31.35° elevation from O1's position at time of the photographs in Figure 1. From O2's position the top of that same green picket was angularly coincident with HD 156629, which was at 297.67° azimuth and 51.00° elevation. Each of these angles define a ray pointing away from their observer. These rays nearly intersect (their closest point separated by 0.5 km) around 51.49° N, 121.00° W, at 145-km altitude.

A comparison of pairs of rays was not possible for Steve as it is lacks sufficient structure to identify common features between the two observers. Instead, the boundaries of Steve identified in O2's photograph were used to define two surfaces: the northward and southward boundaries of Steve. In contrast, the stars identified in O1's photograph mark the upper and lower boundaries of Steve. We then estimated the altitude range of Steve by calculating the positions at which the upper and lower rays passed through the northward and southward boundaries of Steve. For example, the westmost bottom edge of Steve marked with a empty triangle in Figure 1a is angularly coincident with the star HD 183369 from O1's perspective, which was at 217.62° azimuth and 29.63° elevation from O1's position at time of the photographs in Figure 1. Starting from O1's position, this ray crossed the northern boundary of Steve (as defined by O2's photograph) at 51.62° N, 121.04° W, at 129-km altitude and crossed the southern boundary of Steve at 51.3251° N, 121.376° W, at 155-km altitude. The average of these two positions results in an altitude estimate of 142 ± 13 km.

3. Results

Based on the methodology described in the previous section and as shown through Figure 2, our estimates for the altitude of the bottoms of the pickets range is between 92 and 97 km while the tops are from 141- to 153-km altitude. Note that the uncertainty in the individual altitude determination is less than the variation in the mean altitude. The dominant source of uncertainty stems from the uncertainty of the pickets' precise location, owing to their inherent thickness, which is approximately 5 km. We propagated this 5-km uncertainty in the meridional position of the picket fence through the triangulation calculations described above, which results in an altitude uncertainty of roughly 2 km. The altitude uncertainty caused by the 1-min uncertainty in the timing of the photographs is less than 100 m and is negligible. We note that the pickets shown in Figure 2 are horizontally separated from one another by between 15 and 25 km, with an average spacing of 18 km.

Our estimates of the lowest boundary of Steve range from 141 to 151 km. The estimates for its upper boundary range from 226 to 249 km. Due to the meridional thickness of Steve from O2's perspective, there is a 20-km uncertainty in the meridional location of the bottom of Steve and a 35-km uncertainty in the meridional location of the top of Steve. When we propagate these meridional uncertainties through our triangulation calculations, our altitude estimates have uncertainties in altitude of roughly 15 km for the lower boundary and 30 km for the upper boundary of Steve.

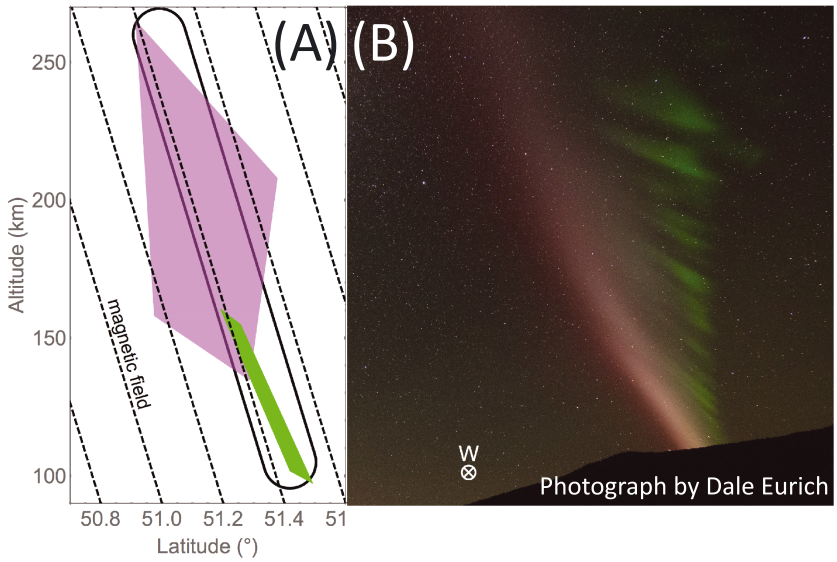

Figure 3. (a) In purple quadrilateral, area within which Steve has to be located, based on the triangulation of photographs shown in Figure 1. In narrow green quadrilateral, estimated boundaries of the picket fence. (dashed lines) Projection of the local magnetic field. (closed black contour) Possible overall area over which Steve and the picket fence would overlap through common magnetic field lines. (b) A westward facing photograph of Steve taken around 05:44 UT on 16 September 2017 by Dale Eurich (O3). Westward direction labeled with W.

The source of the more considerable uncertainties in the altitude estimates of Steve is better understood when observations are plotted in latitude and altitude, as shown in Figure 3a. The purple quadrilateral shown in this figure marks the region within which we estimate Steve to be. As O1 simply provides an upper and lower boundaries and O2 provides a northward and southward boundaries for the phenomenon, all we can ascertain is that Steve is within this quadrilateral. The size of the quadrilaterals in Figure 3 represent the uncertainty in the position triangulation of Steve and the picket fence. However, quite remarkably, we note that in Figure 3a, the upper-southern corner of the purple quadrilateral, the lower-northern corner of the quadrilateral, and the estimated location of the picket fence (shown in green) are all basically aligned and that the angle of that line is consistent with the angle of the Earth's magnetic field at the location of the observations, as shown as a series of black dashed lines in Figure 3. It is a sensible assumption that the green pickets each roughly trace the Earth's magnetic field as they appear to be caused by precipitating electrons. The precise alignment of Steve and the picket is difficult to discern because of the significant uncertainty in the location of Steve. However, Figure 3 shows that Steve and the picket fence are within 0.3° (35-km separation) of each other. In Figure 3b, we show a photograph by O3 of the Steve event looking westward around 05:44 UT, roughly 10 min prior to the photographs shown in Figure 1. As this photograph was not taken at the same time as the others, it does not directly improve our triangulation of Steve or the picket fence. However, it provides a different observation angle than the other photographs and is qualitatively consistent with Steve and the picket fence extending up and southward along similar magnetic field lines.

We can estimate the altitude range of Steve far more precisely under the assumption that it extends along the Earth's magnetic field. Under this assumption, O2's northward boundary of Steve corresponds to O1's lower boundary, and O2's southward boundary corresponds to O1's upper boundary. The results of this calculation are shown as an axis superimposed on a portion of O1's photograph, shown in Figure 4a. The additional constraint of the Earth's magnetic field does not change the estimated altitude for the picket fence but extends the altitude range of Steve to between roughly 130 and 270 km with faint emissions visible up to 300 km. The dominant source of uncertainty for the altitude estimates shown in Figure 4 stems from the fuzzy boundary of Steve which results in an uncertainty in altitude of approximately 2 km, similar to the uncertainty in the altitude of the picket fence discussed above. We separated the red, green, and blue channels for each pixel in the photograph shown in Figure 4a and show the median brightness of those channels for each row of pixels in Figure 4b. The *y* axis of this figure is scaled to match the pixel rows in Figure 4a. We note that the picket fence is seen primarily in the green channel of the photograph, while Steve is seen in all three channels. At higher altitudes, the relative brightness of the red channel of Steve appears to increase, which is also

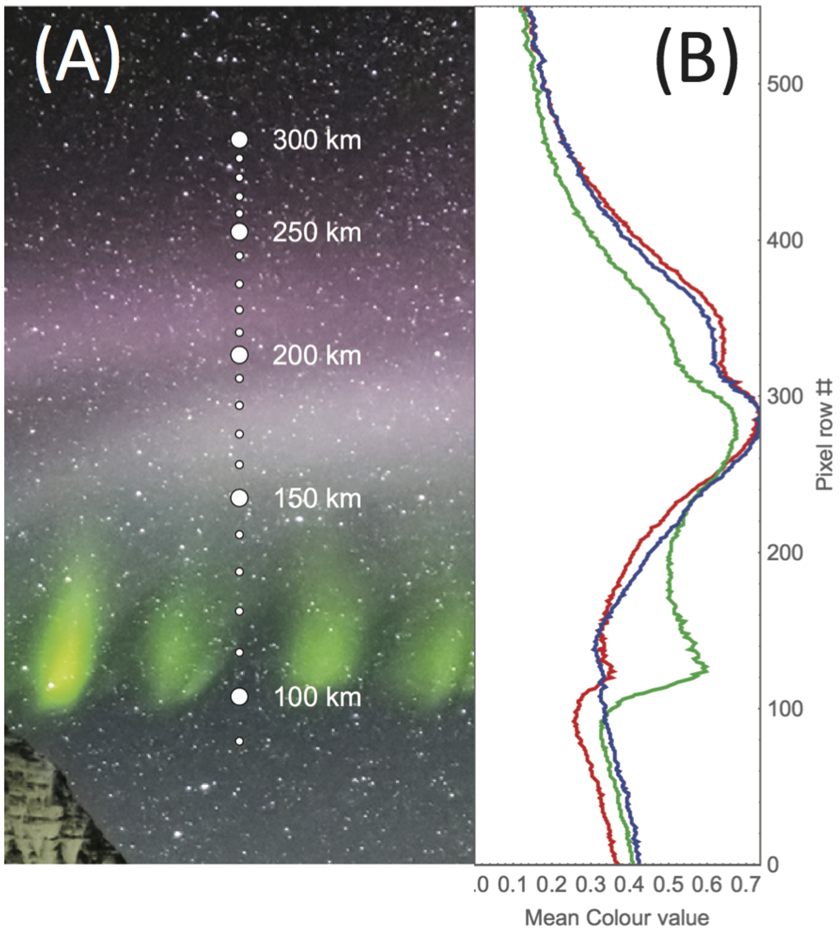

Figure 4. (a) Altitude profile retrieved for Steve and picket fence under the assumption that both phenomena extend along the Earth's magnetic field. The altitude markers are superimposed on a section of Robert Downie's (O1) photograph already shown in Figure 1. (b) Mean red, green, and blue normalized channel brightness for each row of pixels of the image shown in (a). The *y* axis of this figure is scaled to match the pixel rows in (a).

seen in Figure 4a where Steve has a red appearance above roughly 200 km. These qualitative observations should, however, be interpreted with caution as the photographs presented in this study have not been color calibrated for scientific purposes.

4. Discussion and Conclusions

By triangulating observations of Steve and the green picket fence structure from 16 September 2017, we estimate the picket fence to range from roughly 95- to 150-km altitude and Steve to range from roughly 130- to 270-km altitude. Additionally, we find Steve and the picket fence to align with each other along similar magnetic field lines. These altitude estimates are consistent with the picket fence being caused by precipitating electrons, as suggested by Nishimura et al. (2019) and Gillies et al. (2019). This stated that it is currently unclear what source of precipitation is responsible for these green bands spaced roughly 18 km apart, moving steadily westward equatorward of the aurora at between 200 and 300 m/s. It is interesting to note as well that if the two phenomena are exactly field aligned with one another, this has significant consequences on the ionospheric electrodynamics of Steve. Steve appears to be colocated with intense SAID occurring in unusually deep midlatitude density troughs (Archer et al., 2019). Electron precipitation in this region (associated with the picket fence) would significantly enhance the local plasma density, resulting in higher conductivity and lower plasma velocities. As such, the exact relative location of Steve and the picket fence is a significant detail that should be determined precisely in future studies.

Steve is largely above the picket fence and is located in the lower *F* region. Gillies et al. (2019) describe known sources of airglow, which typically peak in brightness around 100-km altitude, as potentially responsible for

the visual continuum of Steve. If these chemiluminescent reactions (such as those presented by ; Evans et al., 2010, or ; Hedin et al., 2012) are responsible for the optical signatures of Steve presented in this study, they are much brighter than typically reported and are occurring well above their typical altitude range. Clearly, there is unforeseen chemistry at work here. Large upflows like those reported by Nishimura et al. (2019), which are a known signature of SAID (Anderson et al., 1991), may also play a significant role in unusual ionospheric conditions resulting in Steve. We presumably need to find a chemiluminescent reaction that can create a continuum in the visual part of the spectrum ranging, this between 130- and 270-km altitude.

Acknowledgments
Unaltered digital copies of all images used in this study are available online (doi:10.5683/SP2/1VPEFE). William Archer was supported by grants from the European Space Agency and the Natural Sciences and Engineering Council of Canada. We would like to thank the Alberta Aurora Chasers (AAC) for facilitating this research. It is through the AAC that we identified a suitable event for study and were able to contact the photographers. We hope to continue working with this enthusiastic community in the future.

References

Anderson, P. C., Heelis, R. A., & Hanson, W. B. (1991). The ionospheric signatures of rapid subauroral ion drifts. *Journal of Geophysical Research*, *96*, 5785. https://doi.org/10.1029/90JA02651

Archer, W. E., Gallardo-Lacourt, B., Perry, G., St-Maurice, J.-P., Buchert, S. C., & Donovan, E. (2019). Steve: The optical signature of intense subauroral ion drifts. *Geophysical Research Letters*, *46*, 6279–6286. https://doi.org/10.1029/2019GL082687

Cole, K. D. (1965). Stable auroral red arcs, sinks for energy of Dst main phase. *Journal of Geophysical Research*, *70*, 1689–1706. https://doi.org/10.1029/JZ070i007p01689

Evans, W. F. J., Gattinger, R. L., Slanger, T. G., Saran, D. V., Degenstein, D. A., & Llewellyn, E. J. (2010). Discovery of the FeO orange bands in the terrestrial night airglow spectrum obtained with OSIRIS on the Odin spacecraft. *Geophysical Research Letters*, *37*, L22105. https://doi.org/10.1029/2010GL045310

Gallardo-Lacourt, B., Liang, J., Nishimura, Y., & Donovan, E. (2018). On the origin of STEVE: Particle precipitation or ionospheric skyglow? *Geophysical Research Letters*, *45*, 7968–7973. https://doi.org/10.1029/2018GL078509

Gallardo-Lacourt, B., Nishimura, Y., Donovan, E., Gillies, D. M., Perry, G. W., Archer, W. E., et al. (2018). A statistical analysis of STEVE. *Journal of Geophysical Research: Space Physics*, *123*, 9893–9905. https://doi.org/10.1029/2018JA025368

Gillies, D. M., Knudsen, D., Donovan, E., Jackel, B., Gillies, R., & Spanswick, E. (2017). Identifying the 630 nm auroral arc emission height: A comparison of the triangulation, FAC profile, and electron density methods. *Journal of Geophysical Research: Space Physics*, *122*, 8181–8197. https://doi.org/10.1002/2016JA023758

Gillies, D. M., Knudsen, D., Donovan, E., Jackel, B., Gillies, R., & Spanswick, E. (2019). First observations from the TREx spectrograph: The optical spectrum of STEVE and the Picket Fence phenomena. *Geophysical Research Letters*, *46*, 7207–7213. https://doi.org/10.1029/2019GL083272

Hedin, J., Rapp, M., Khaplanov, M., & Stegman, J. (2012). Geophysicae observations of NO in the upper mesosphere and lower thermosphere during ECOMA 2010. *Annales Geophysicae (November)*, *30*, 1611–1621. https://doi.org/10.5194/angeo-30-1611-2012

Hirsch, M. (2016). pymap3d, Boston, MA.

Kozyra, J. U., Valladares, C. E., Carlson, H. C., Buonsanto, M. J., & Slater, D. W. (1990). A theoretical study of the seasonal and solar cycle variations of stable aurora red arcs. *Journal of Geophysical Research*, *95*, 12,219–12,234. https://doi.org/10.1029/JA095iA08p12219

MacDonald, E. A., Donovan, E., Nishimura, Y., Case, N. A., Gillies, D. M., Gallardo-lacourt, B., et al. (2018). New science in plain sight: Citizen scientists lead to the discovery of optical structure in the upper atmosphere. *Science Advances*, *4*(March), 16–21. https://doi.org/10.1126/sciadv.aaq0030

Mathematica (2017). Wolfram Research, Inc., Champaign, IL.

Nishimura, Y., Gallardo-Lacourt, B., Zou, Y., Mishin, E. V., & Knudsen, D. J. (2019). Magnetospheric signatures of STEVE: Implication for the magnetospheric energy source and inter-hemispheric conjugacy. *Geophysical Research Letters*, *46*, 5637–5644. https://doi.org/10.1029/2019GL082460

SkySafari Corp. (2019). Simulation curriculum, Minnetonka, MN.

Weber, E. J., Buchau, J., Moore, J. G., Sharber, J. R., Livingston, R. C., & Reinisch, B. W. (1984). F layer ionization patches in the polar cap. *Journal of Geophysical Research*, *89*, 1683–1694. https://doi.org/10.1029/JA089iA03p01683

Weber, E. J., Klobuchar, J. A., Buchau, J., & Carlson, H. C. (1986). Polar cap F layer patches: Structure and dynamics. *Journal of Geophysical Research*, *91*, 121–129. https://doi.org/10.1029/JA091iA11p12121

Appendix C: Neutral densities and BCBF

Birkeland Current Boundary Flows (BCBF) are narrow channels of fast-moving plasma which occur at the boundary between the Region 1 (R1) and Region 2 (R2) current systems. Archer et al. [2016] observed BCBF with the Swarm satellites and found them to be a persistent feature of northern (winter) hemisphere near midnight during geomagnetically quiet conditions. They hypothesize that these narrow flow channels are a natural consequence of Birkeland current closure through ionospheric Pedersen currents during geomagnetically quiet conditions. Under such conditions, the ionospheric height-integrated conductivity can vary by several orders of magnitude between the regions of upward and downward field-aligned current (FAC), resulting in large electric fields (and plasma flows) in the downward current sheets.

Extreme ionospheric plasma conditions and typically associated with geomagnetic activity. However, as BCBF are a quiet-time phenomenon and can persist for several hours, they allow extreme plasma to be studied in relatively steady conditions. For example, Archer et al. [2015] investigated extreme and anisotropic plasma heating associated with a BCBF (although not called a BCBF in that publication) in which ionospheric temperature was enhanced by a factor of 10 perpendicular to the local magnetic field, while remaining relatively unchanged parallel to the local magnetic field. Recently, Fenrich et al. [2020] (manuscript under revision) investigated the spatial and temporal variations of two BCBF events using both SuperDARN and the Swarm satellites. They found the narrow flow channels observed by the Swarm satellites to be coincident with field line resonances (FLRs) with periods on the order of 30 minutes and electric field amplitudes on the order of those of the BCBF.

Because BCBF are defined in part by large electric fields that persist for several hours, the neutral atmosphere is likely influenced through frictional heating and subsequent upwelling as well as neutral winds. However, the neutral particle densities and flows associated with BCBF have not yet been investigated largely due to limited instrumentation available to do such an analysis. Unfortunately, the acceleration measurements from the Swarm satellites exhibit several artifacts and can be difficult to interpret. Siemes et al. [2016] outline that the most prominent disturbances in the Swarm accelerometer measurements (ACC) are “slow temperature-induced bias variations and sudden bias changes”. They also describe a four-stage data processing strategy used to calibrate the accelerometer measurements into scientifically useful neutral density estimates.

Following the work of Siemes et al. [2016] we have roughly calibrated Swarm C accelerometer measurements surrounding a BCBF event. We find measurements consistent with neutral density upwelling as well as neutral winds. However, the position and orientation of these accelerometer signatures relative to the coincident Swarm electric field measurements are not simple or intuitive. In particular, the apparent neutral upwellings are observed poleward of the electric field maxima, and the neutral winds are not always parallel to the local plasma flow. These results highlight the complex relationship between the ionosphere and the co-located neutral atmosphere.

Period of interest

In this study we investigate Swarm satellite measurements from 18 December 2013. During this period of time, the polar orbit of the Swarm satellites were in a “pearls on a string” orientation and passed through the winter (northern) auroral oval around magnetic noon and midnight. The magnetic local time (MLT) of the Swarm satellites vary by a few hours over a given day. As they passed from pre to post-midnight on 18 December 2013 the Swarm electric field instruments (EFIs) measured both eastward and westward flows, consistent with a typical 2-cell convection pattern.

Two orbits during the period of interest observed particularly narrow and intense flow channels around 12.5 and 17.2 UT (shown in Figure 1). These flow channels meet the criteria for BCBF. This study aims to complement the electric field, magnetic field, plasma density, and electron temperature measurements from the Swarm satellites with neutral density perturbation and neutral wind estimates.

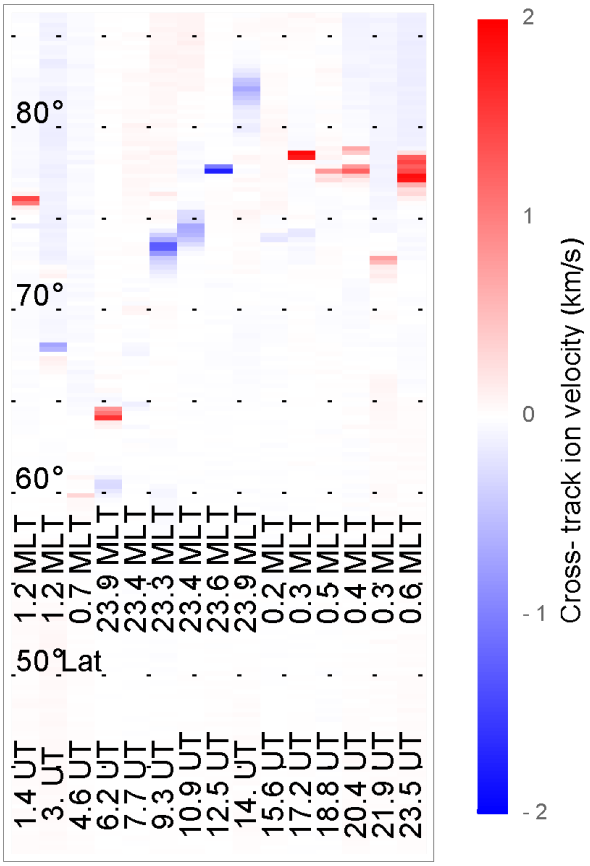

Figure 1: Swarm A EFI cross-track flow estimates from 18/12/2013. Positive (red) ion velocities are roughly eastward.

Methodology

The dominant feature of the along-track Swarm C accelerometer measurements is a single discontinuity observed around 9.8 UT. This discontinuity was easy to identify as it occurred over only 5 s in which the along-track accelerometer measurements jumped by over 5 $\mu m/s^2$, which is several orders of magnitude larger than any apparently geophysical variations. Having resolved the discontinuity, the along-track accelerometer measurements qualitatively match the large-scale acceleration estimates from precise orbital determination (POD). We calibrated the accelerometer measurements by matching their first and second moments to those of the POD acceleration estimates, illustrated in Figure 2.

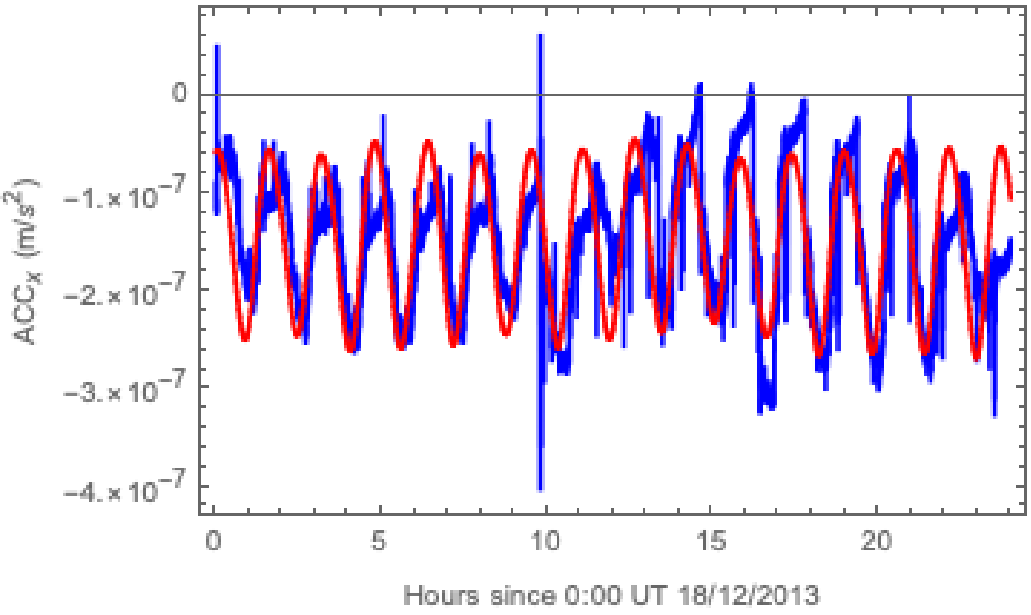

Figure 2: Swarm C along-track acceleration estimated by precise orbital determination (red) and scaled Swarm vector accelerometer measurements.

Note that this deviates from the methodology of Siemes et al. [2016], who instead calibrate the accelerometer measurements independently from POD and then validate their results with the POD estimated acceleration. The methodology used in this study ignores important effects such as that of temperature on the Swarm accelerometers over the period of interest. However, in this study we seek only a rough calibration of the ACC. Furthermore, Siemes et al. [2016] report that typical fluctuations in ACC due to temperature occur on the scale of half an orbit, while the features investigated in this study span only a few hundred km.

We have limited this study to Swarm C ACC because the Swarm A and B large-scale along-track ACC variations do not agree with POD acceleration estimates. However, Figure 1 shows Swarm A EFI estimates because Swarm C EFI was cycled off around 17.5 UT during the period of interest. As stated above, these two satellites were in similar orbits during the period of interest, and while both Swarm A and C EFI were operating they qualitatively agreed with one another.

In this study we do not calibrate cross-track ACC, as there are no clear trends in large-scale cross-track POD acceleration estimates with which to compare them. Instead, once we resolved measurement discontinuities (at the same timestamp as for along-track ACC), we subtracted the ACC baseline and normalized the estimates so that the maximum absolute value of the cross-track ACCs are 1. As such, cross-track ACC estimates shown in this study are a qualitative estimate of acceleration perturbations.

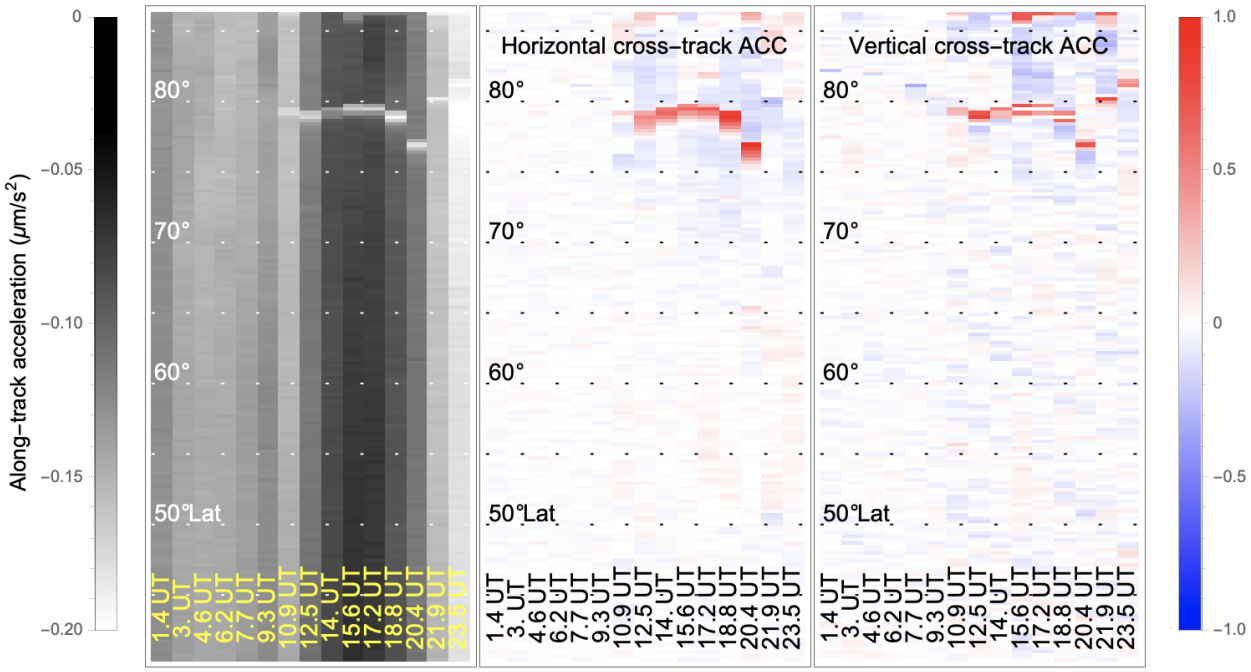

Figure 3: Swarm C acceleration estimates for 18 December 2013. Cross-track acceleration estimates are represented in normalized units.

A summary of the Swarm C ACC estimates for the period of interest, shown in Figure 3, reveals an increased negative along-track acceleration as well as cross-track acceleration in narrow features between 75° and 80° latitude from 12.5 UT to 21.9 UT. These features are roughly coincident in space and time with the narrow flow channels shown in Figure 1. To better understand how these acceleration estimates contribute to the overall understanding of this event, we now present all available plasma parameters for the two orbits with largest plasma flows. Namely, those around 12.5 and 17.2 UT.

Results

The cartesian coordinate system employed in this discussion is as follows. The x-direction is defined by the anti-ram vector of the satellite, which during this period is roughly northward. The z-direction is parallel to zenith. Therefore, the y-direction is “to the right” in the satellite-frame which is roughly westward for these measurements. The Swarm crossing of the BCBF during the 12.5 UT orbit (Figure 4) shows a north-westward flow-channel co-located with the Region 2 downward current sheet, typical of the pre-midnight sector. The relative magnitude of the westward and northward component of the plasma flow is unknown as the along-track flows are uncalibrated. However, the satellite appears to be passing through the R1/R2 current roughly 45° relative to the current sheets as the x and y component of the magnetic perturbations are roughly equal. This suggests that the x and y components of the plasma flow are also roughly equal.

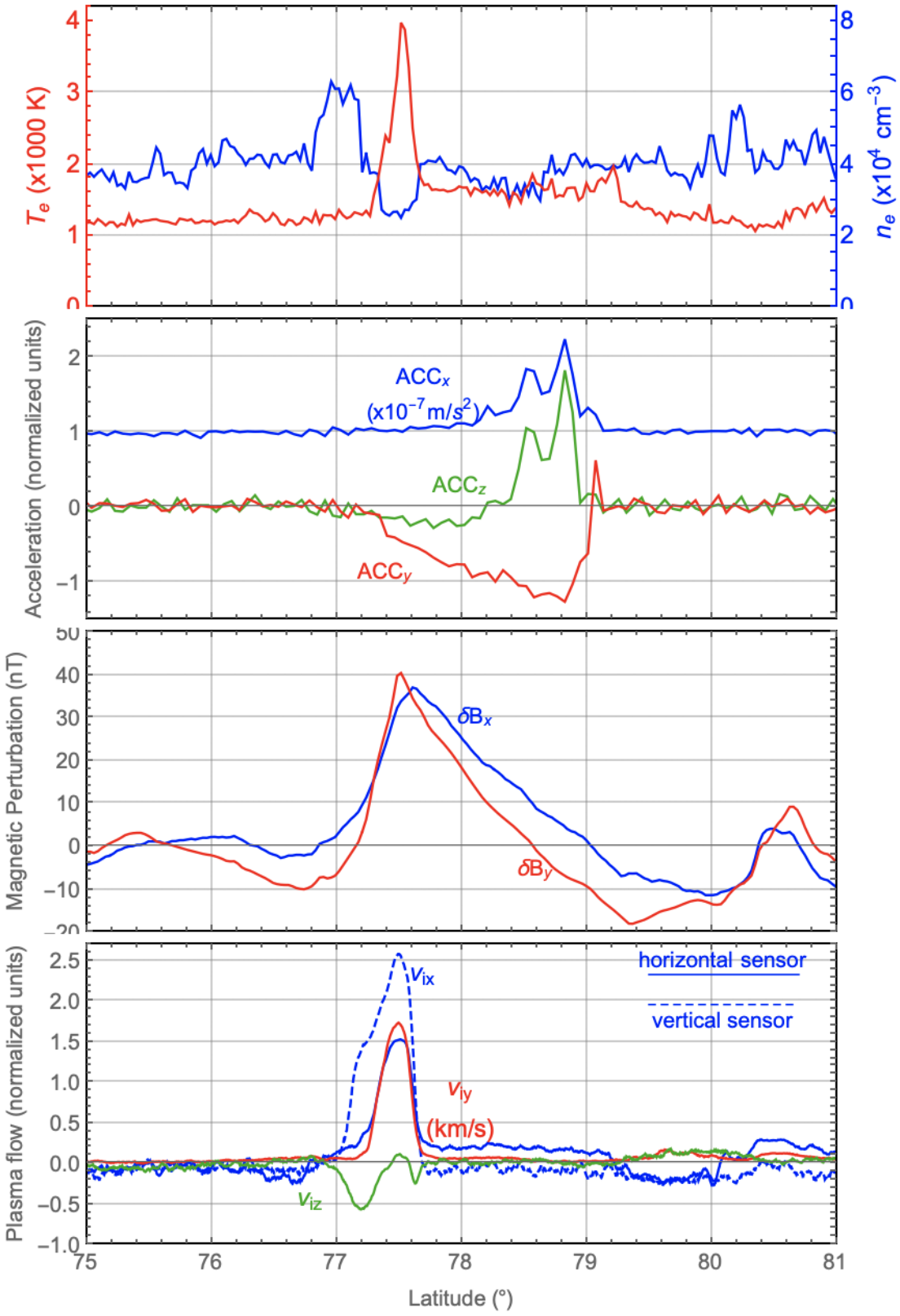

Figure 4: Plasma and neutral atmosphere parameters surrounding the narrow flow channel for the Swarm C orbit around 12.5 UT on 18 December 2020.

Note that two v_{ix} estimates are shown in Figure 4. This is because there are two thermal ion imager (TII) sensors as part of the EFI that each sample the ion velocity distribution in planes perpendicular to one another. As a result, they each provide an independent estimate of the along-track (x) plasma velocity.

Offset from the north-westward plasma flow is a region of downward flowing ions. This is atypical of BCBF, which are often associated with upflows. It is possible that this downflow represents ions falling back down after previously upwelling due to the BCBF. Co-located with the BCBF is a electron temperature enhancement of several thousand degrees as well as a plasma density depletion. This density depletion may result from electrons being evacuated up the field-line in order to carry the downward R2 current.

The Swarm accelerometer measures an enhancement in along-track acceleration roughly 100 km poleward of the peak plasma flow. This doubling of northward acceleration is consistent with roughly a doubling of the local neutral density, or alternatively, some combination of neutral-density enhancement as well as along-track neutral flow. Co-located with the apparent neutral-density enhancement is a region of upward acceleration, with a smaller-magnitude downward acceleration immediately equatorward. We observe an eastward acceleration over the entire ~200 km region that includes both the plasma flow channel and neutral density enhancement.

In the 17.2 UT BCBF crossing (Figure 5), the Swarm satellites were in the post-midnight region. As a result, the BCBF is eastward, and co-located with the R1 downward current sheet. For this event the Swarm satellite appears to pass though the R1/R2 currents at roughly 60° relative to the current sheets as the y-component of the magnetic perturbation is roughly double that of the x-component. Consistent with this, the ratio of v_{iy} to v_{ix} is larger in Figure 5 than in Figure 4.

Again, we observe a region of downward flowing plasma associated with the BCBF, however the ~3 km/s offset in vertical plasma flow poleward of the BCBF should be disregarded as it is likely an artifact. We also observe a region of enhanced electron temperature co-located with the BCBF, but do not observe as clear a density depletion in Figure 5 as was seen in Figure 4.

The accelerometer measurements are also very similar from Figure 4 to 5. There is once again a region of apparent neutral density enhancement and upward neutral wind roughly 100 km poleward of the BCBF, as well as an eastward acceleration spanning the 200 km that encompass the BCBF and the density enhancement. However, in Figure 5 we observe no region of significant downward acceleration.

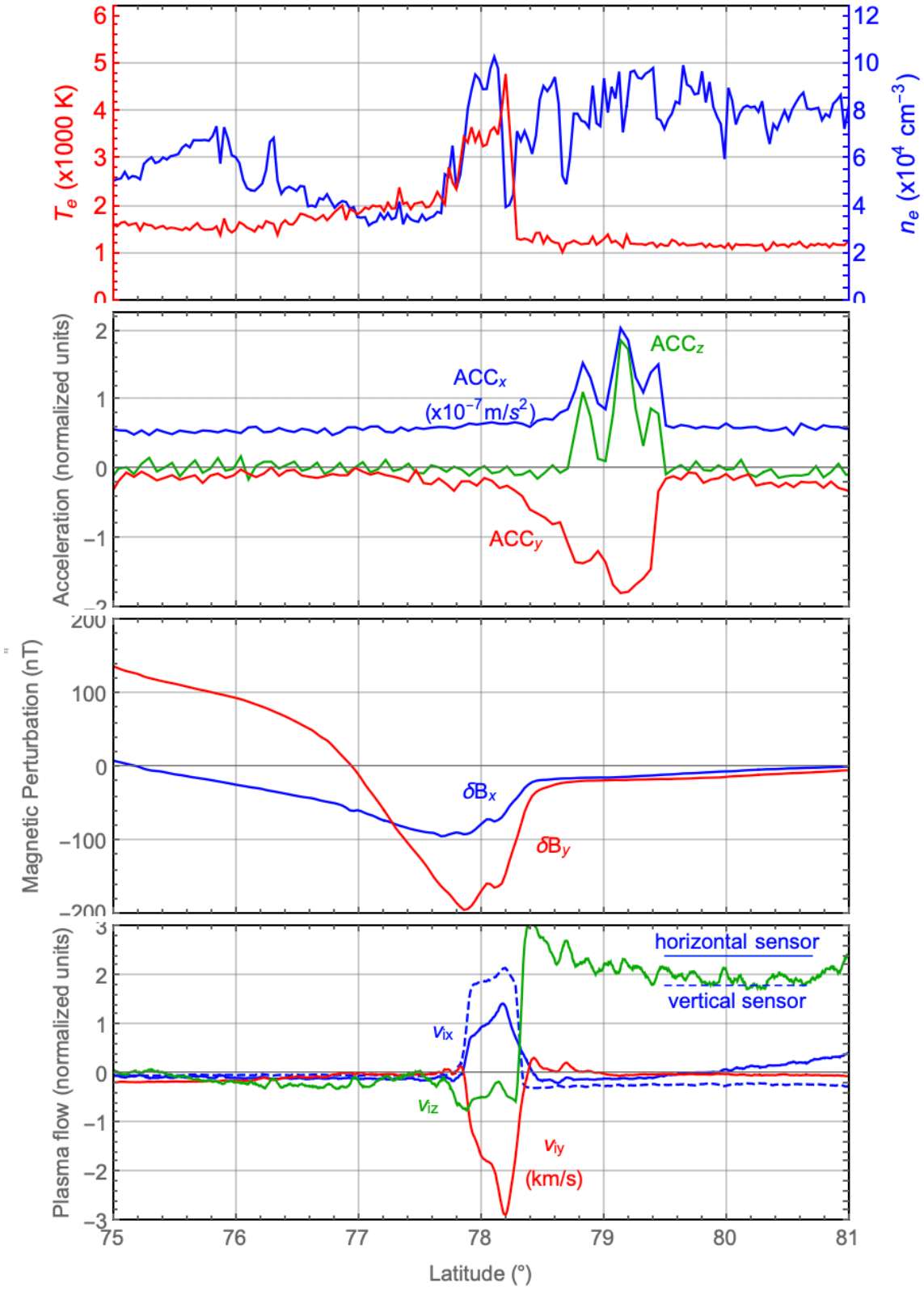

Figure 5: Plasma and neutral atmosphere parameters surrounding the narrow flow channel for the Swarm C orbit around 17.2 UT on 18 December 2020.

Discussion and Conclusion

A simple expectation of these BCBF events is that frictional heating would result in the neutral atmosphere upwelling and winds coincident with the peak plasma flow. The expected ACC observations would be acceleration in the positive x-direction, the positive z-direction, and the y-direction parallel to the horizontal plasma flow. The mysteries to be solved regarding the observations shown in Figures 4 and 5 are therefore:

- Why are neutral density enhancements observed more than 100 km poleward of the peak plasma flow?
- Why is the ACC_y perturbation negative in both Figures 4 and 5, when v_{iy} is positive in Figure 4 and negative in Figure 5?

One possible explanation for the location of the neutral density enhancement that can be immediately elimination is the tilt of the local magnetic field. Neutral upwelling would occur roughly vertically, while the electric field (and plasma flow) enhancement follows the background magnetic field. As such, we would expect the neutral density enhancement poleward of the peak electric field when observed from above the region of frictional heating. However, even if we assume that the heating region is around 100 km altitude this effect can only account for at most a ~50 km separation between the peak plasma flow and density enhancement.

Another explanation of these observations is that the plasma flow changes almost immediately with changes in plasma flow, which neutral upwelling and winds will change relatively slowly. This is somewhat supported by the consistency of the location of the acceleration perturbations observed by Swarm (Figure 3), which change significantly less from orbit-to-orbit than the measured plasma flow (Figure 1). However, this would imply that it is coincidence that we observed a density enhancement poleward of the peak plasma flow in both Figure 4 and 5.

An alternative explanation is that the neutral density upwelling not caused by frictional heating. Instead, it may be caused by the significant electric field gradient of the region. In steady state the neutral atmosphere is traveling anti-sunward through the polar cap, dragged by anti-sunward traveling ions. The transition from anti-sunward flow to north-west and north-eastward flow (in Figures 4 and 5 respectively) may be sufficiently drastic to effectively compress the neutral atmosphere, causing it to upwell.

Regarding the sign of the ACC_y perturbations, no clear explanation is apparent at this time. The neutral winds when observed above the region where they were created can be seen as occurring in the past as it takes time for the upwelling neutral particles to reach (in this case) Swarm altitude. Such an effect could result in westward neutral winds observed post-midnight, as when those winds were created their geographic location was pre-midnight. However, in Figures 4 and 5 we observed eastward flows both pre- and post-midnight.

It should be noted that the Swarm satellites were traveling anti-sunward (from north to south) for the events studied in this manuscript. This is relevant because the ACC perturbations are observed before any strong signature in plasma velocity or electron temperature, making it seemingly impossible for the ACC perturbations to be an artifact resulting from the instrument entering extreme plasma conditions. Moving forward, this work would benefit greatly from the involvement of the Swarm ACC team with the following goals:

- To confirm that the ACC perturbations presented in this study do not match any known artifacts in the ACC data products.
- To determine whether official calibration of the ACC data for the period of interest is warranted.
- To solicit any additional insight they may have on the unintuitive observations presented in this manuscript.

Appendix D:

Investigation of highly correlated electric and magnetic perturbations as observed by the Swarm satellites on 26/02/2014.

In this study we investigate the ionospheric plasma signatures of a unique event as measured by the Swarm A and C satellites. In this event, which was observe 26 February 2020, the electric and magnetic perturbations are highly structured and unusually highly correlated with one another.

Observations

Both Swarm A and C were in similar dawn-to-dusk orbits when crossing the northern hemisphere in late February 2014. They both observed highly structured electric and magnetic perturbations when crossing the auroral zone and polar cap, shown in Figures 1 and 2.

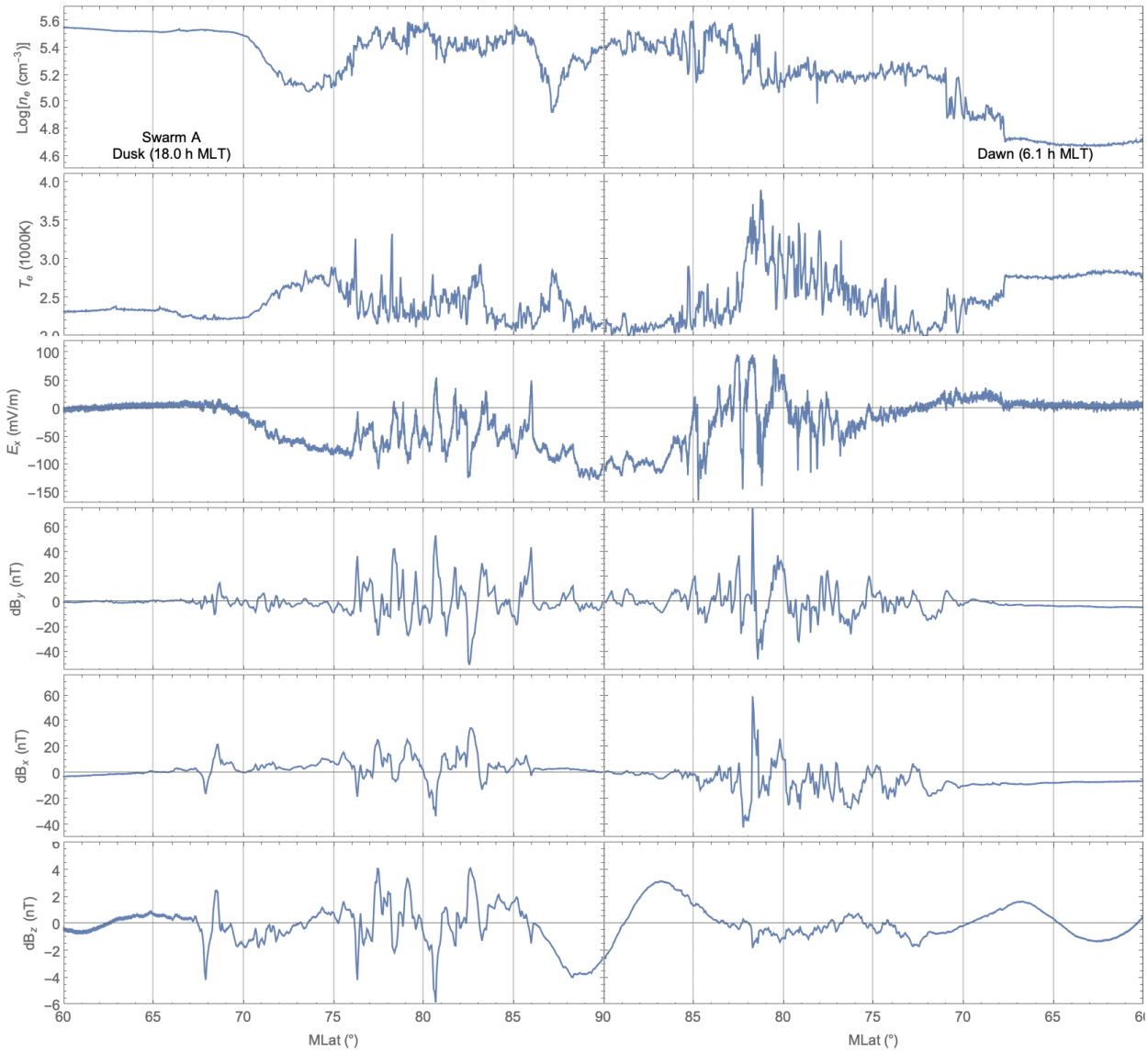

Figure 1: Swarm A measured plasma parameters for the auroral northern hemisphere high-latitude crossing around 22 UT on 26/02/2014.

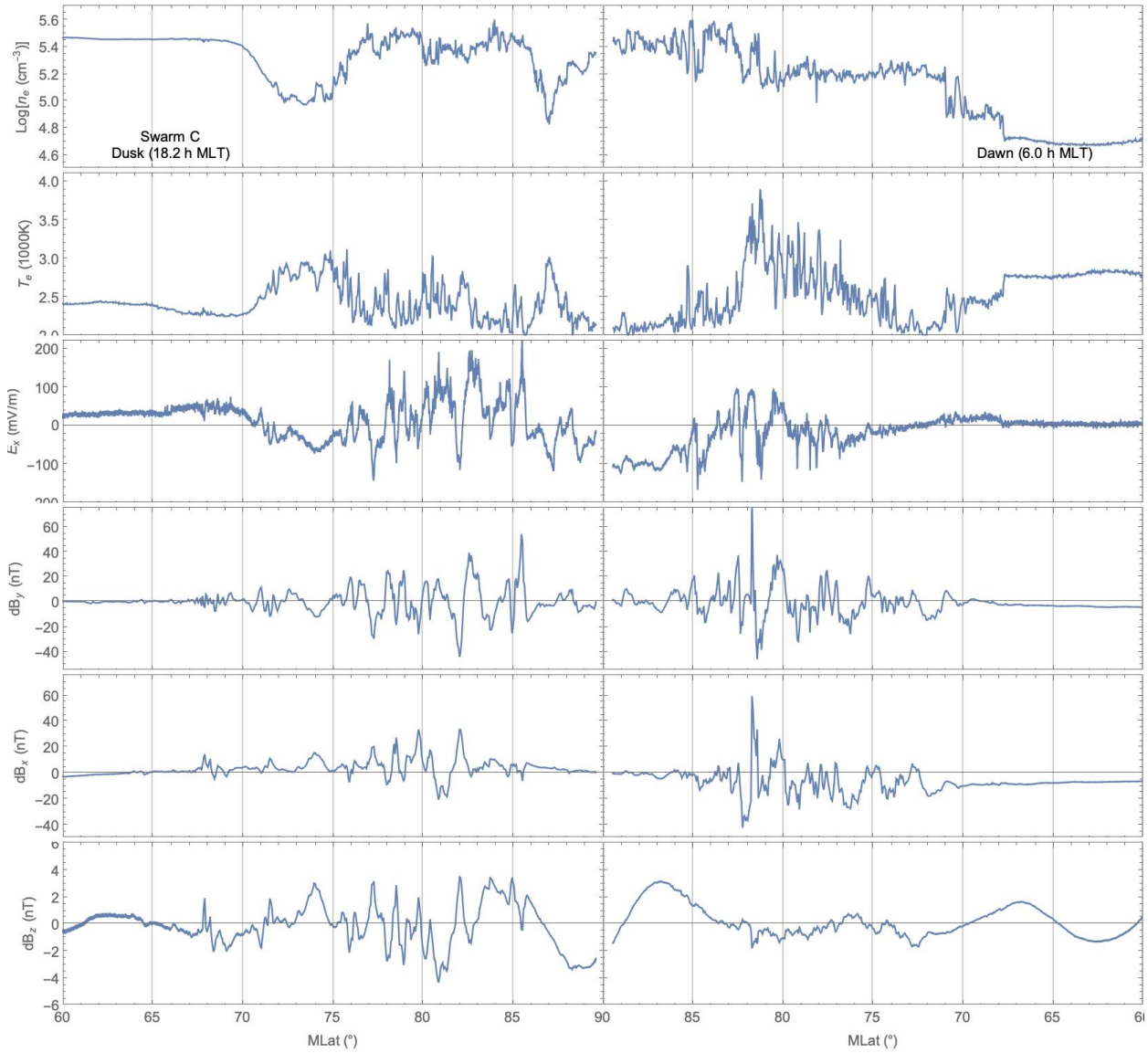

Figure 2: Swarm C measured plasma parameters for the auroral northern hemisphere high-latitude crossing around 22 UT on 26/02/2014.

The measurements shown in Figures 1 and 2 are qualitatively very similar to one another, with most differences between the two observations likely due to ionospheric dynamics acting on the 10-minute separation between the two satellite orbits. One significant difference between Figures 1 and 2 is the magnitude of E_x perturbations, which were measured by Swarm C to be ~1.5 times larger than those measured by Swarm A. We believe at this time that this difference is due to instrument error on the part of Swarm C, but more investigation is required.

We re-plotted some of these observations with axes that emphasize some of the interesting characteristics of this event, focusing on 75-85° magnetic latitude (MLat) in Figures 3 and 4. The top panels of these figures illustrate how highly correlated dB_y and dE_x are for this event. We subtracted a 1000-point running average from both quantities, which corresponds to ~1 minute of measurements which span ~4° of MLat. These two quantities have a correlation of 0.94 over the entire window shown in Figure 3. Spectrograms of dB_y and dE_x with a 1-minute sliding sampling window unsurprisingly show very similar Fourier coefficients except for the 0^{th} term because of the large-scale electric fields observed by Swarm. These spectrograms show the absolute values of the Fourier coefficients of the corresponding plasma parameters. We find the dominant wavelength to be ~140 km observed by Swarm A, and 210 km observed by Swarm C.

In Figures 3 and 4 we also investigate the ratio of dEx and dBy in two different ways to determine if this electromagnetic signature is Alfvenic in nature. The ratio of the absolute values of the dominant Fourier coefficients are shown in blue (in the 4^{th} panel from the top). The slope of the linear best fit of dEx and dBy over a 1000 point (1-minute) sliding window is shown in red. These two estimates both result in a ratio of dEx and dBy of roughly 1.5 km/s over the entire region of interest. This is roughly triple the local Alfven speed as estimated by local plasma parameters (shown in green, 4^{th} panel from the top).

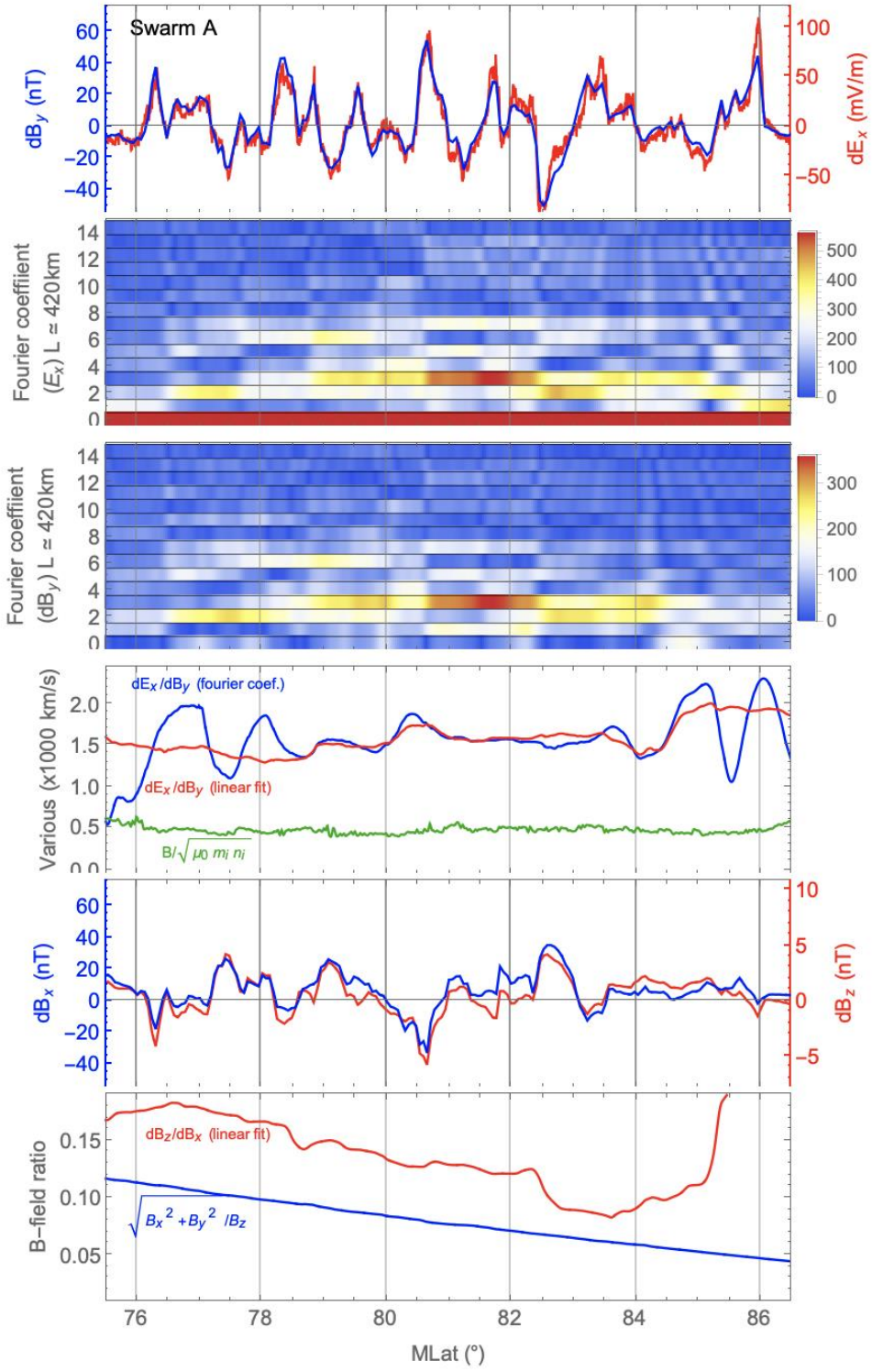

Figure 3: Various derived quantities from the Swarm A northern-hemisphere dusk crossing around 22 UT on 26/02/2014.

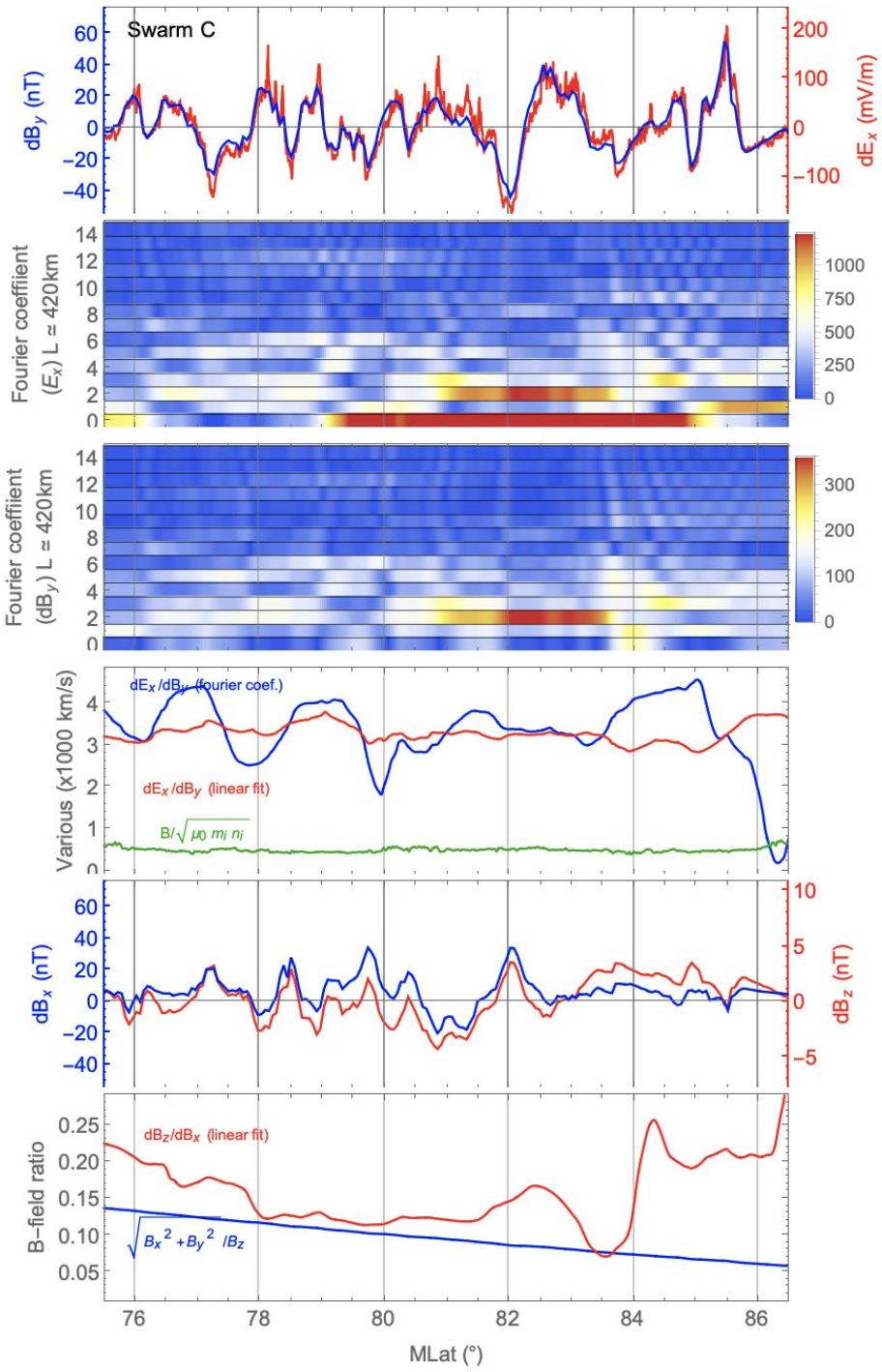

Figure 4: Various derived quantities from the Swarm C northern-hemisphere dusk crossing around 22 UT on 26/02/2014.

Finally, we illustrate in the bottom two panels of Figures 3 and 4 that the small dB_z perturbations observed are likely dominated by magnetic perturbations perpendicular to the local magnetic field. We show this by first illustrating that dB_x and dB_z are highly correlated, then show that the relative magnitude of dB_x and dB_z change with magnetic latitude in a way that is consistent with the change in magnetic dip angle. dB_z/dB_x deviates from this pattern above 84° MLat, however this ratio is based on near-zero values above 84° MLat and should likely be disregarded.

Interpretation of electric and magnetic fields

There is some ambiguity to the physical interpretation of these electric and magnetic measurements. The typical interpretation of satellite-measured magnetic perturbations is that they are caused by the satellite traveling through regions of field-aligned current (FAC). Often this description is further simplified to assume that the satellites are passing through (and normal to) semi-infinite planes of FAC. If we also assume that these currents connect to one another below the satellite through Pedersen currents, then the ratio of dE_x and dB_y is relates to the height-integrated Pedersen conductivity of the region. Under this interpretation, the high correlation between dE_x and dB_y implies a constant Pedersen conductivity over the dusk-side auroral oval. This is somewhat surprising as upward FAC is assumed to be carried by downward traveling energetic electrons that would increase the plasma density at lower altitudes and as such modify the local Pedersen conductivity. Such a constant Pedersen conductivity as implied by the above Swarm observations is unusual in such a highly structured (and likely dynamic) region. Additional careful analysis is required if this interpretation is to be put accepted.

Alfven waves are another potential source of in-phase structured electric and magnetic perturbations. Under this assumption, the relatively constant ratio of dE_x and dB_y represents a constant Alven speed over the region of interest. However, the Alfven speed estimated by electric and magnetic fields is roughly triple that estimated by local plasma density, background magnetic field, and assuming a plasma dominated by O^+. Knudsen et al. [1990] point out that the ratio of electric and magnetic fields can vary with altitude if Alfven waves reflect off of a large conductivity gradient (such as the lower ionosphere), forming a standing wave. In such a situation the electric field would minimize and the magnetic field would maximize near the point of reflection, with the opposite being true one-quarter wavelength up the standing wave. However, larger scale Alfven waves (such as would cause signatures like those presented in this study) have periods on the order of ten minutes and wavelengths of tens of thousands of kilometers. As such, Swarm observations are very close to the reflection surface and we would therefore expect the electric perturbations to be (if anything) suppressed rather than enhance. As a side note, these signatures would be considered Alfvenic rather than magnetosonic, as the magnetic perturbations appear to be entirely perpendicular to the background magnetic field.

Future Work

The ionosphere is a complicated and dynamic system, often resulting in observations that are difficult to interpret. Events such as those presented in this report provide a measure of clarity due to the simplicity of some aspect of the observations. The implication of such clean measurements is that we are observing a scenario that is well described by relatively simple approximations. Deviations from those simple approximations are easy to identify and can lead to further insight into the physics of the situation. As is apparent from my discussion above, additional analysis is required to confidently interpret this case study. This analysis will also inform the insights that can be gained from investigating this event.